Liquid residence time distribution in micro-reactors with complex geometries

By Alexandra Hopley

Thesis submitted to the Faculty of Graduate and Postdoctoral Studies as required for the degree of Master of Applied Science

In

Department of Chemical and Biological Engineering Faculty of Engineering

uOttawa

University of Ottawa

Abstract

Micro-reactors, enabling continuous processes at small scales, have been of growing interest due to their advantage over batch. These advantages include better scaling, as well as improved mass and heat transfer, though many new challenges arise due to the small scales involved such as non-negligible entrance effects and significant pressure drops.

The flow in coils, rectangular channel serpentine plates, mix-and-reside plates, and complex liquid-liquid mixing plates was investigated and characterized using residence time distribution (RTD) tests. A pulse test was used to determine the RTD curve shape of these reactors at flowrates ranging from 20 to 100 g/min. A semi-empirical, multi-parameter model was used to describe the asymmetrical curves, while the axial dispersion model was used to describe the symmetrical ones.

The Peclet number is given in function of the Reynolds number for the liquid-liquid plates that were found to be near-plug flow (Pe > 100). In a continuous mixing plate, the Pe ranged from 190 to 475 with Pe increasing as Re increased. The effect of straight channel sections in micro-reactors is also evaluated. Longer straight segments between micromixers resulted in the development of unidirectional flow and the occurrence of tailing in the RTD.

Finally, the suitability of a liquid-liquid plate for a reactive liquid-solid system is evaluated. The plugging is determined visually and by measuring pressure increase; pressure started to increase after 5 minutes and the experiment had to be halted after 10 minutes due to plugging. Parallels between the particle size distribution and the residence time distribution curves are drawn. The particle size distribution of silver chloride at low flow rates is much wider

than at high flowrates. The average particle size at high flowrates was also much lower (≈69nm) than at low flowrates (≈112nm).

Table of Contents

List of Figures

List of Tables

1 Introduction

1.1 Background

Micro-reactors are used for production of milligrams [1] to kilograms [2] of product per day as well as the steps in between. This makes them suitable for preclinical and clinical development in the pharmaceutical industry. During this time, new products are continuously produced and tested. As a result, modular setups are used, allowing for flexibility, speed and scalability. [3] While small-scale batches are highly flexible, the transition from batch to continuous production has been of growing interest in the pharmaceutical industry [4].

At production scale, discontinuous processes are expensive to run, partly due to vessels and equipment needing to be emptied and decontaminated between batches. Continuous processes require less human intervention and cleaning steps, resulting in less product losses, time losses, and use of water/cleaning supplies than batch processes. [5] Reduced handling also reduces potential safety hazards of the process. Safety is further increased by requiring smaller equipment and generally having better control over process parameters such as temperature and pressure. [6] Overall, transitioning to continuous processes increases efficiency and decreases cost, particularly as the process is scaled-up [5]. It is reported that if continuous production is desired at large production scale, it is better to start with continuous production at bench-scale [7].

Process scaling via both numbering-up (adding identical reactors in parallel) and sizing-up (increasing channel size and reactor volume) micro-reactors has been studied. Su et al. explored the numbering-up method for a photochemical reaction where sizing-up would have impeded the “homogenous irradiation of the entire reaction medium” [8]. However, sizing-up is often more

practical than numbering-up reactors [7]. It is therefore the ability to size-up micro-reactors while maintaining efficient heat and mass transfer that makes this technology so much more attractive than batch processes.

Micro-reactors have efficient heat transfer due to their high surface to volume ratios [9] which comes from having a small hydraulic diameter [10]. Increased heat transfer is especially important with highly exothermic reactions and/or heat sensitive products [2]. To avoid temperature spikes, the maximum diameter can be calculated based on an overall heat transfer coefficient, heat of reaction and rate of reaction. The heat transfer coefficient is a combination of the convective resistance of the reactive medium, the wall resistance, contact resistance, and convective resistance of the thermal fluid. [10]

Micro-reactors have short diffusion paths therefore it is widely assumed that they have good radial mixing when calculating conversion profiles, although this is not quite accurate [9]. Mixing strategy is one of the key issues with micro-reactors. At this scale, creating turbulence cannot be achieved purely by increasing flow rate as it results in pressure drops that are too high for most pumps. This is because the pressure drop is proportional to $\sim 1/d_t^5$ in turbulent flow. To induce radial mixing at more achievable flow rates, one of two mixing strategies are employed: active or static mixing. Mixing using external sources, such as vibrations, impellers, or pulsing, is defined as active mixing. Static mixing takes advantage of the flow energy, inducing mixing using specialized channel design. [11]

The reactors studied in this paper use static mixing, specifically, curvature, expansion/contraction, and obstacles for changes to the velocity field magnitude and direction. The purpose of these geometries is to generate chaotic secondary flow patterns, thereby causing

reactants to more rapidly come into contact [12]. This is important because local concentrations have effects on selectivity and reaction rate [13]. However, mixing happens at different scales and is conventionally divided into micromixing, mesomixing, and macromixing [14].

i. *Micromixing* or molecular mixing occurs in large part at the Batchelor scale, which is defined as:

$$\eta_B = \eta_K Sc^{-\frac{1}{3}} \tag{1}$$

Diffusion only becomes significant at this scale and leads to the homogenization of the mixture. [15]

ii. *Mesomixing* occurs at the Kolmogoroff scale, at which energy is dissipated by the viscous forces, and is defined as [15]:

$$\eta_K = \left(\frac{\nu^3}{\Psi}\right)^{0.25} \tag{2}$$

iii. *Macromixing* occurs over the entire reactor volume and is associated to the flow regime and patterns within the reactor [14].

Just as with macro-scale channels, flow regime is determined by the Reynolds number

$$Re = \frac{u d_t \rho}{\mu} \tag{3}$$

using the hydraulic diameter d_t and with transition between the laminar and turbulent flow regimes occurring at Re between 2000 and 4000 for a straight channel [16]. It should also be noted that the flow pattern is dependent on the vessel geometry while flow regime is not.

Therefore when referring to a laminar flow regime, it is understood that the Re is below 2000; referring to a laminar flow pattern means that the fluid has a parabolic profile [14].

1.2 Motivations and Research Topic

While micro-reactor technology in general has advantages over batch technology, there is an array of commercially available micro-reactors, not all of which will be appropriate for a particular application. Plouffe et al. developed a toolbox approach for choosing micro-reactors. This approach involves first determining the rate of reaction which has been divided into three categories. Type A reactions have reaction rates of milliseconds to seconds and are therefore, in general, mass transfer limited. Reactors with rapid mixing and heat transfer are most appropriate. Type B reactions have a reaction rate of several seconds to minutes and are therefore largely kinetically rate limited when in single phase. While good heat transfer and mixing may still be required at the entrance of the reactor, the appropriate reactors must have enough volume to allow the reactions to come to completion. Type C reactions have a reaction rate of several minutes to hours. Reactions of this type especially benefit from increased temperature and pressure control as a means to safely increase the reaction rate. [17]

The second consideration of the Plouffe et al. approach is the phases involved. For a single phase, a mix-and-reside approach is suggested. For an immiscible liquid-liquid system, phases can separate if left to reside, therefore continuous mixing is suggested. When dealing with gas-liquid systems, higher pressure is favourable and mixing methods which break up gas bubbles are used at the entrance of the reactor. In solid-liquid systems, reactors which are not prone to plugging are used. [17]

While this approach does not take into consideration every important aspect, it does offer a concrete starting point when choosing a micro-reactor for a particular application. This method has been expanded upon, taking into consideration heat transfer and mesomixing [12][10]. This paper expands on this method, exploring the macromixing aspect.

Macromixing is measured using residence time distribution (RTD) [14]. Knowing the RTD can help predict yield and diagnose problems in reactor operations [18]. Furthermore, Kuan et al.'s [19] work with secondary flow in twisted pipes in the laminar regime indicates that heat transfer, mass transfer, and RTD are linked and can be optimized simultaneously. RTD is therefore useful to determine the appropriateness of a particular micro-reactor for a specific application when examined in conjunction with other characteristics.

What is typically desired when examining macromixing is a narrow and symmetrical RTD. In this condition, each molecule spends close to the same amount of time in the reactor; this allows more control on the yield of the reaction. Broader RTD curves are indicative of ineffective contacting and a lower conversion can therefore be expected; this affects concentrations and selectivity [18]. The flow pattern associated to a narrow, symmetrical RTD is plug-flow, theoretically defined as having a radial velocity profile that is a straight line, across the entire pipe. To achieve near-plug flow conditions, good radial mixing is required, and axial dispersion must be minimized. Axial dispersion is the longitudinal spreading of a section of fluid, independently of molecular diffusion; small axial dispersion is indicative of near plug flow conditions [20]. Levenspiel defines small axial dispersion as $D/uL < 0.01$ [20].

Residence time distribution, and by extension dispersion, is usually determined by measuring the concentration of a tracer at the exit of the reactor as a function of time [18].

Bošković and Loebbecke [21] used a spectroscopically measured dye impulse successfully obtained distinguishable RTD curves for various "split and combine" micro-mixers. Many others [22] [23] measured Peclet numbers for a plate and coil micro-reactor using a step approach, but the pulse approach is preferred when experimentally possible because the step approach can hide some effects such as channeling and tailing [20].

Many of the works that have explored RTD in micro-reactors focus on modeling to describe the flow behaviour. Nieves-Remacha et al. [24] conducted an analysis of flow regimes and patterns in a reactor with heart-shaped cells at various flow rates using computational fluid dynamic simulations. Bošković et al. [21] used a quasi-Newton method to fit Ham and Platzer's [25] four parameter semi-empirical model to asymmetrical distributions and the dispersion model to symmetrical distributions.

The objective of this work is to characterize the RTD of commercial micro-reactors using a similar method that has been used for the geometries mentioned above. Serpentine, mix-then-reside, and continuous mixing plates will be compared with attention on the effect of straight channel sections on the RTD in micro-reactors. The parallels between RTD and particle size distribution will be explored in Chapter 4 using a crystallization reaction.

1.3 Nomenclature

$C(t)$	Concentration, arbitrary units
D	Effective dispersion coefficient, $m^2 s^{-1}$
D_{ax}	Axial dispersion, $m^2 s^{-1}$
d_t	Hydraulic diameter (taken at the smallest cross-section), m
$E(t)$	Exit age distribution as a function of time, s^{-1}
$E(\theta)$	Exit age distribution as a function of dimensionless time
f_i	Model estimation
L	Characteristic length, m
N	Number of CSTRs in series
$Pe = uL/D$	Peclet number
Q	Volumetric flow rate
R	Coil radius, m
R^2	Coefficient of determination
$Re = \rho\, d_h\, u/\, \mu$	Reynolds number
$Sc = \mu/\, \rho\, D$	Schmidt number
SS_{res}	Residual sum of squares
SS_{tot}	Total sum of squares
s^3	Skewness
t	Time, s
t_B	Breakthrough time, s
t_m	Mean residence time, s
t_{max}	Time at maximum absorbance, s
u	Mean fluid velocity, $m\ s^{-1}$
V	Volume
y_i	Observed data
η_B	Batchelor scale, m
η_K	Kolmogoroff scale, m
ν	Kinematic viscosity, $m^2 s^{-1}$
Ψ	Rate of energy dissipation, $W\ kg^{-1}$
$\Theta = t/\tau$	Dimensionless time
μ	Dynamic viscosity, Pa s
ρ	Density, $kg\ m^{-3}$
σ^2	Variance, s
σ^2/τ^2	Dimensionless variance
τ	Nominal space time, s

2 Experimental

2.1 Experimental setup

The RTD for each micro-reactor was determined using a pulse experiment where a fluorescein tracer was injected at the inlet of the reactor, and detected at the outlet using an optic sensor. A schematic of the experimental set up is shown in Figure 1. The deionized water feed was pumped by a micro-gear pump (HNP) controlled using a flow meter (Coriolis, Promass) connected to a HiTech Zang lab manager and software.

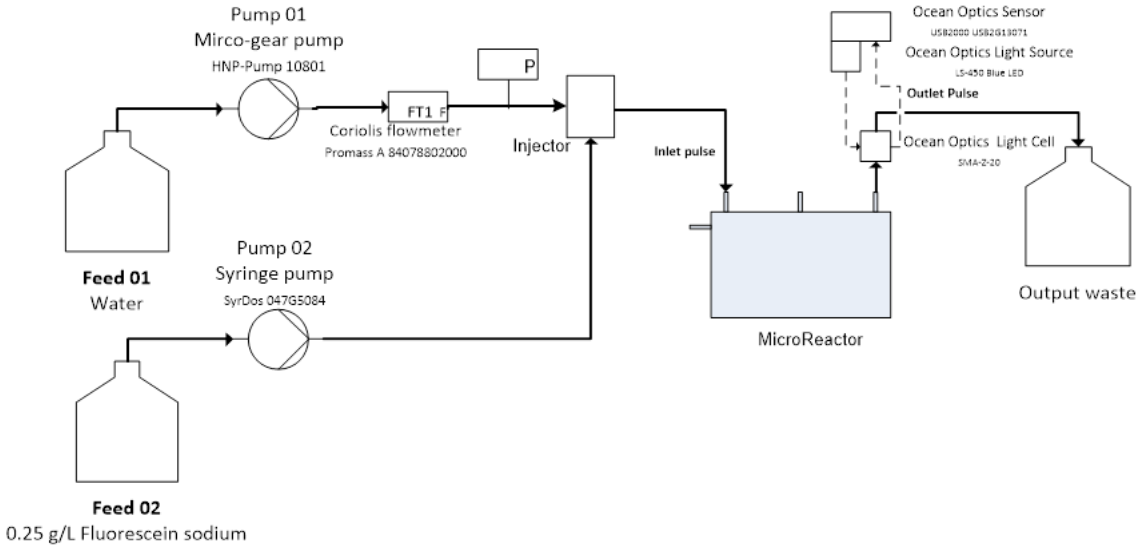

Figure 1 – Experimental setup

Multiple injection methods were tested within this setup. This included the commonly used method of an HPLC valve [21], but the flow rates were too high and the switching severely disrupted the overall flow and gave a multi-peaked pulse. The method which was the least disruptive to the pulse and which gave the most consistent result was to send a fixed volume of tracer dye using a pre-set volume setting on the pump. The pulse was sent at rate of 15 mL/min

using a syringe pump (SyrDos) equipped with two 2.5 mL syringes. The resulting pulse was consistent when the line leading to the injector was thoroughly flushed with the tracer dye as seen in Figure 2. The inlet pulse signal was measured at each flow rate prior to experiments. These signals were used in further calculations as to not require an additional spectrometer at the reactor entrance, which would add volume and noise.

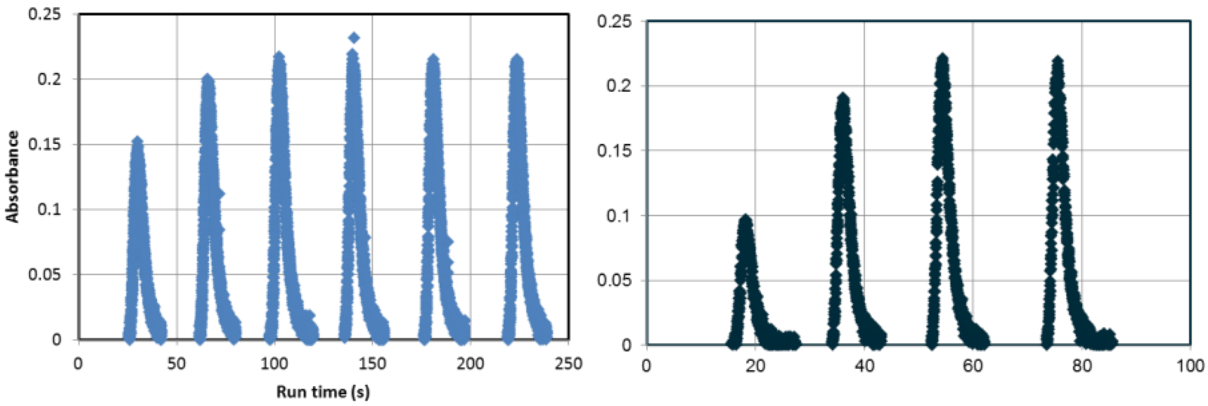

Figure 2 – Pulse absorbance with pre-set volume setting on the syringe pump at a system flow rate of 50 g/min (left) and 100 g/min (right) without line being flushed (first 2 pulses) and with line being flushed (subsequent pulses) with tracer dye.

The tracer dye pump and the line leading up to the injector were kept above the injector and this line had a 1/16” tube diameter to help keep the line flushed with tracer dye. This capillary, shown in Figure 1, also injected the dye into the main flow channel as to create a plane across the entire flow profile. The entrance of the plates and the connecting tubing had 1/8” tube diameter. The coils and the connecting lines had 1/4” tube diameter. The number of expansions and contractions were minimized to avoid unnecessary disruption of the pulse prior to the reactor.

The tracer was a 0.25 M fluorescein sodium (CAS No. 518-47-8) solution in deionized water. Its solubility in water is high (500 mg/mL) while its molecular diffusivity in water is low

(4.2 x 10^{-10} m^2/s) which is why it is often used in RTD experiments [26]. It was estimated that any adsorption to the wall, if present, was minimal and did not significantly alter results. Both feeds were connected to a tee (the injector), shown in Figure 3, through which the 0.04 mL dye pulse was sent perpendicular to the flow of water. This pulse volume and concentration were chosen because they resulted in a single-peaked pulse, shown in Figure 4, with time spread below the theoretically acceptable 5% of the total residence time. Furthermore, these allowed a pulse that was detectable by the spectrometers at all tested flow rates without oversaturating them.

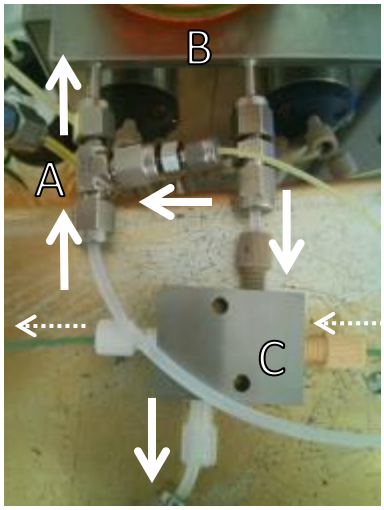

Figure 3 – A) Fluorescein dye injected into the water stream via a Tee, B) A5 micro-reactor plate, and C) light cell attached to tubes (north-south) and optical fiberglass (east-west).

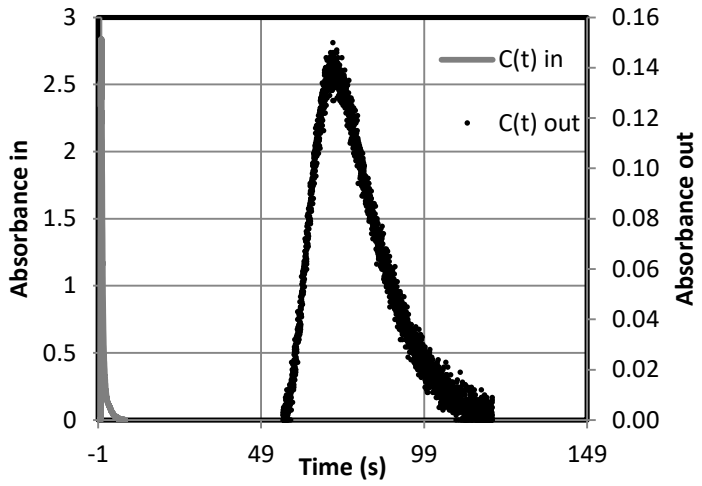

Figure 4 – Inlet and outlet signal response at 15 g/min in an LL plate with grouped mixers (pulse volume = 0.04 mL; dye concentration = 0.25 g/L; injection duration = 160 ms).

At the outlet of the reactor, the pulse was measured in a light cell. The light source was a blue LED (Ocean Optics, LS-450) and the absorption was measured by a sensor (Ocean Optics, USB2000) being read at 460 nm wavelength and at 3 ms integration time by the OceanView software. The Z-shaped light cell (Ocean Optics) was installed as close to the outlet as possible so that the total additional volume was below 0.5 mL (<5%), as seen in Figure 3. The range of concentrations is small and follows Beer's law, as seen in Figure 5. The start time t = 0 was recorded as the time of the pulse at the tee. The volume between the tee and the inlet (0.25 mL) of the reactor was included in the total volume to adjust for the discrepancy.

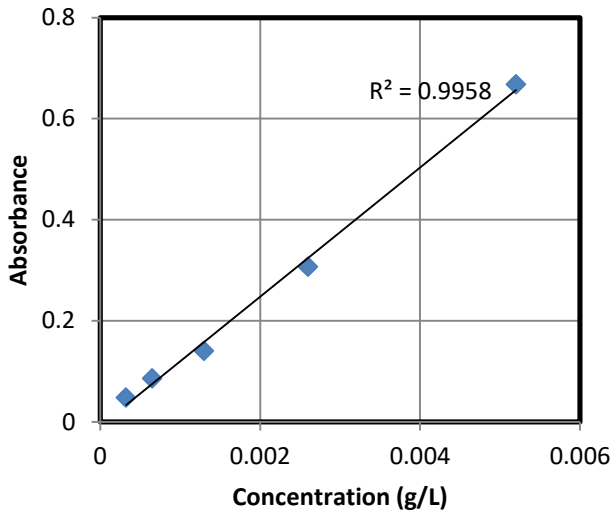

Figure 5 – Dye concentration vs measured absorbance at 50 g/min.

2.2 Micro-reactors Studied

2.2.1 Teflon Reactor Coils

The double vortex (Dean vortex) induced in coils makes them a popular static mixer. Coils were later improved on by combining them with the concept of flow inversion, resulting in coil flow inverters. The effect of RTD shape has been studied for both coil geometries. [27] As a point of comparison, two coils were constructed: a single direction coil and an inverting flow coil. Key to inducing vortices in coils is the ratio between the tube diameter and the coil diameter ($d_t/2R$). This ratio is used to characterize the flow in the coil via Dean's number:

$$De = Re\sqrt{\frac{d_t}{2R}} \tag{4}$$

The tube diameter itself is important as it determines Re. Another consideration for coils is the pitch or torsion, which is the distance between coils. It is preferable for pitch to be minimized because increasing pitch, either by having loose coils or very thick walls, straightens the tube [28]. Additional variables are available for coil flow inverters. Inversion coils typically feature

arms with one or more 90° bends; it has been shown that the RTD narrows with more than three 90° bends [27]. By changing the direction of the centrifugal force, the plane of the Dean vortices is changed, thereby inverting the position of the maximum and minimum axial velocities in the flow [29]. Each arm usually has two or more coil turns on it in order to develop secondary flow. [27]

The RTD depends on Re in certain ranges of these key parameters. For example, Trivedi et al. did not find any clear dependence of Pe on Re for 10<Re<1000 with their coils with very small $d_t/2R$ [30]; Sharma et al. observed a sharp increase in that range with larger $d_t/2R$ but with a stagnation in Pe with an 2000<Re <8000 [27]. It should be noted that the Dean number can also contribute to the flow regime when Re is low. Below De = 40 the flow remains unidirectional. At a critical Dean number, usually around De = 55, the symmetrical double vortex is formed. The critical Dean number depends of the shape of the channel. At De ≈ 70 to De ≈ 100, the vortex begins to undulate (wavy regime) and a split-merge phenomena is present. Above De ≈ 100, that phenomena ends and the first burst of turbulence begin. The vortices begin to twist at De ≈ 120. [31] Turbulent regime is generally accepted to be reached at De > 500 [32].

Circular Teflon tubes with an interior diameter of 3.96 mm and a length of 1.6 m were coiled around a 60 mm pipes to create the coils shown in Figure 6. In order to get a close comparison with the serpentine reactor, the length, volume, and cross-sectional area were chosen to match the plate reactor as closely as possible. It was not possible to match the curvature of the plate, which has tight curves followed by straight channels. The Dean numbers for the coils ($d_t/2R$ = 0.066) are in the range of 30-155 with Re of 120-605.

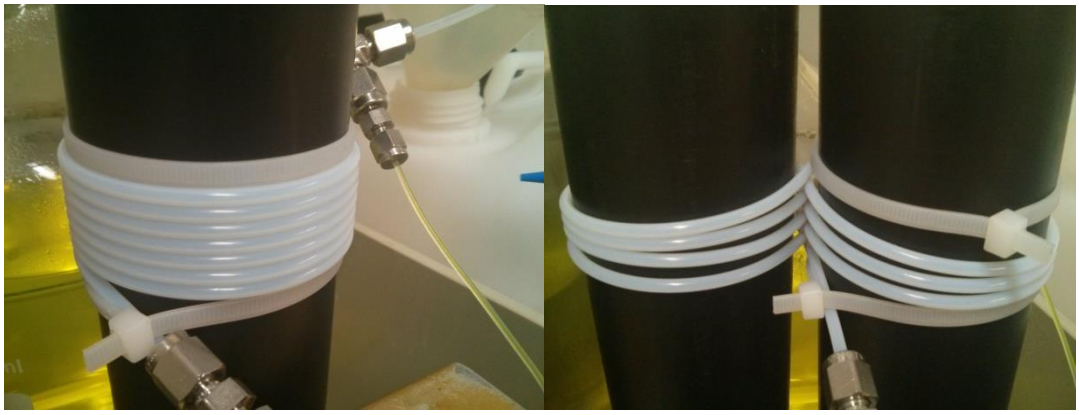

Figure 6 – Teflon coil reactors: single direction coil (left) and figure-8/inverting flow (right).

To mimic the alternating turns on the serpentine plate, the inverted coil studied here was made with a single coil between each turn; the simplest way to construct this was using a figure-8 pattern (180° rather than 90° bends). Note that this design does not allow for minimum pitch, allowing for slight straightening of the tube between turns. Therefore, it is not the most efficient design, but since the primary purpose is to compare the coils to the serpentine plates, the design is adequate.

2.2.2 Micro-reactor Plates

The plate geometries studied are liquid-liquid (LL), serpentine, mix-then-reside SZ, and mix-then-reside tangential (TG). The plates were manufactured by Ehrfeld Mikrotechnik BTS out of a 3.5 mm thick Hastelloy® C22 plate with a 1.5 mm plate welded to the other side. Under typical use, the plates are slid into a rack which also holds heat transfer fluid plates. Drawings of the plates of size-A5, scale-300 are shown in Figure 7. The dimensions of each plate studied are in Table 1.

Table 1 – Micro-reactor plate dimensions.

Plate Design (Figure 7)	Plate name	Smallest mixer dimension (mm)	Largest dimension (mm)	Number of mixing elements	Volume (mL)
A	LL continuous	1.25x0.50	2.0x5.0	223	10.3
B	LL equally spaced	1.25x0.50	2.0x5.0	86	19.5
C	LL grouped spacing	1.25x0.50	2.0x5.0	86	18.8
D	LL minimal	1.25x0.50	2.0x5.0	46	22.2
E	Serpentine 0.5 mm		0.5x10	0	8.26
E	Serpentine 1.0 mm		1.0x10	0	16.27
F	SZ 0.5 mm	0.50x0.28	0.5x10	18.5	8.44
F	SZ 1.0 mm	1.0x0.49	1.0x10	18.5	16.13
G	TG 0.5 mm	0.50x0.20	0.5x10	31	8.3
G	TG 1.0 mm	1.0x0.35	1.0x10	31	15.42

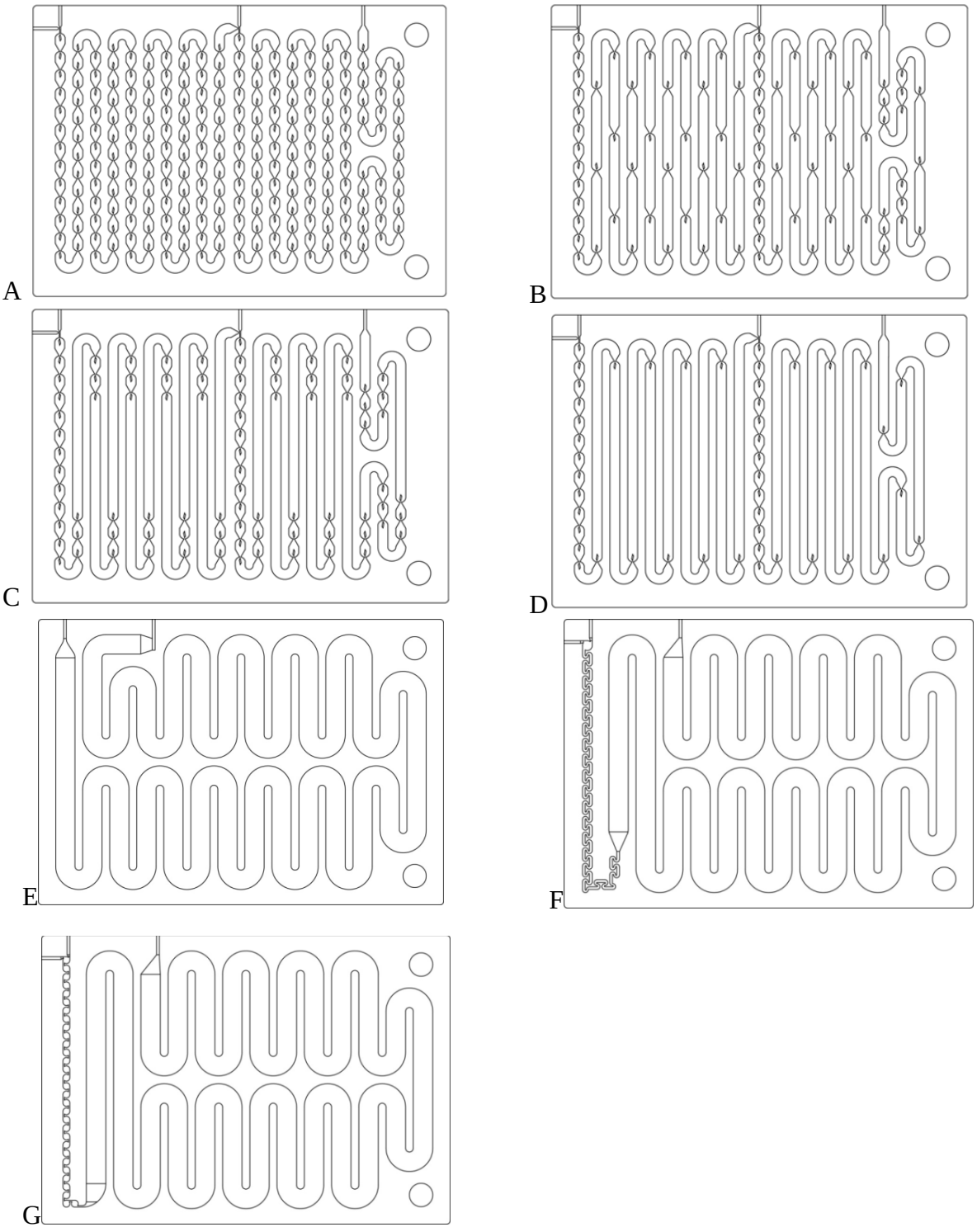

Figure 7 – Micro-reactor plates.

Pressure drop tests were previously performed on these reactors to determine their operational range of flow rates. These LL plates have a range of 15-150 mL/min. The serpentine, SZ, and TG plates have a range of 35-300 mL/min. The pressure drop follows a power law ($\Delta P = KV^n$ where K is a constant and n is 1 in the laminar regime and 2 in the turbulent regime). In this range, the exponent n is indicating transitionary flow for all the plates, as shown in Figure 8: the 1.0 mm Serpentine plate has n = 1.1, the minimally spaced LL plate has n = 1.5, and the continuous plate has n = 1.8.

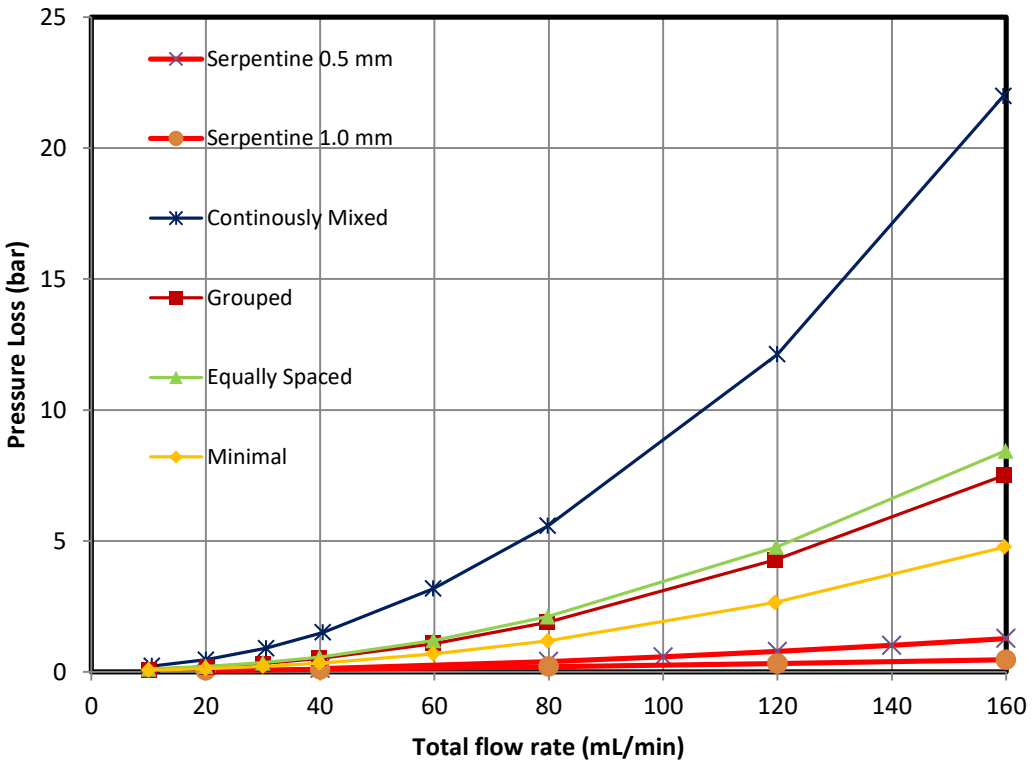

Figure 8 - Pressure loss in LL and serpentine plates

The three mixer geometries which were studied are illustrated in Figure 9. These mixers have been shown to induce mesomixing to various degrees. While the mixer geometry did not affect the overall volumetric mass transfer coefficient in a liquid-liquid drop flow regime at a

given energy dissipation rate, the LL mixer was shown to reach and maintain drop/dispersed flow at much lower flow and energy dissipation rates than the SZ and TG mixers [12]. It was also shown that in a mix-then-reside plate, the main contributor of the pressure loss occurs in the mixing portion .

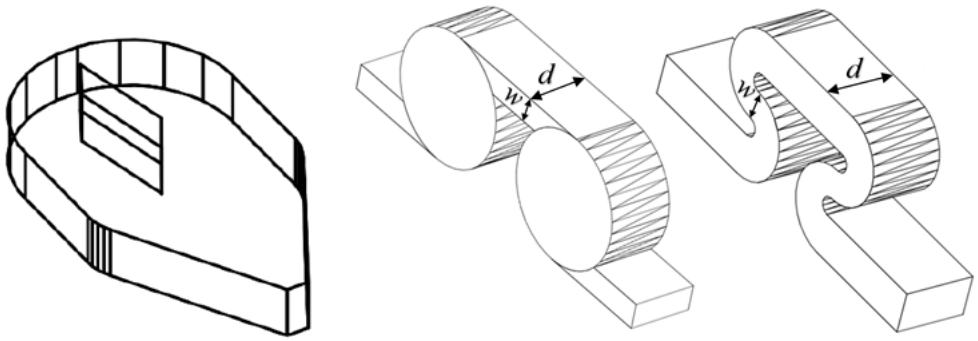

Figure 9 – LL (left), TG (centre) and SZ (right) mixers.

2.3 Data Analysis Method

A common problem which is encountered with RTD analysis is the loss of data at both ends of the response curve due to the cutting of tailing during analysis. To minimize the effect and to allow fair comparison between RTD curves, the same cut-off rule was applied to all data analysis. Firstly, the breakthrough point, t_B, was defined as the earliest time after which no zero-value or negative absorbance measurements are recorded prior to the peak. In other words, between t_B and the RTD peak, no values equal to or below zero were recorded. Similarly, the end point t_{end}, is the latest time after the peak before which negative values are recorded. This method was determined to give the most consistent results but as shown in Figure 10. Furthermore, by calculating the integral of the concentration curve, it was determined that all the fluorscein had exited by the point with an error margin of about 2%.

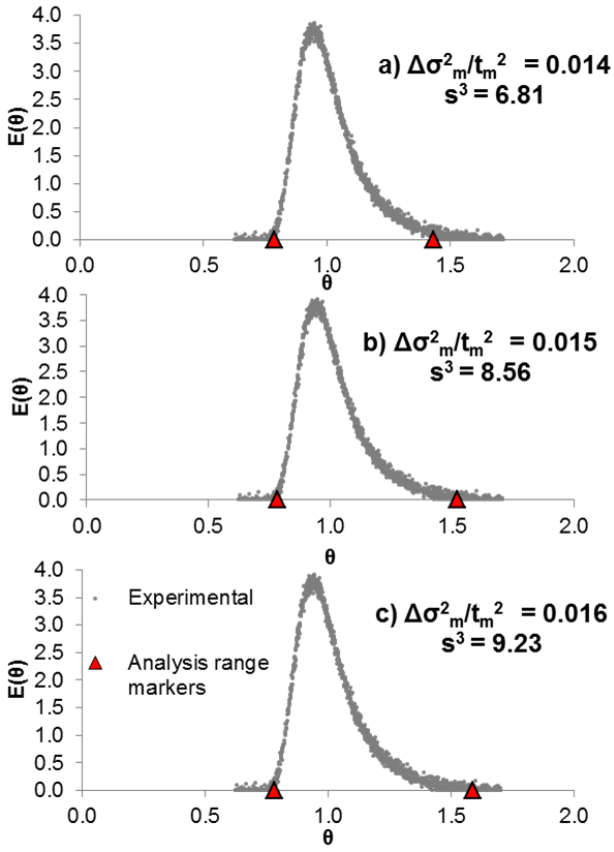

Figure 10 – Effect of analysis cut-off on RTD moments at 42 g/min in an LL plate with grouped mixers at a) first negative (most consistent method), b) first block of 3 negatives, c) about half the values are negative.

Another consideration when analyzing RTD data is that the time of the maximum peak, t_{max}, the calculated mean residence time t_m, and the nominal space time, τ, can but do not necessarily occur at the same time as seen in Figure 11. The maximum peak is equal to the mean residence time only if the curve is perfectly symmetrical; tailing shifts t_{max} to the left. The mean residence time differs from the nominal space time when dead-zones, recirculation, or jetting occurs.

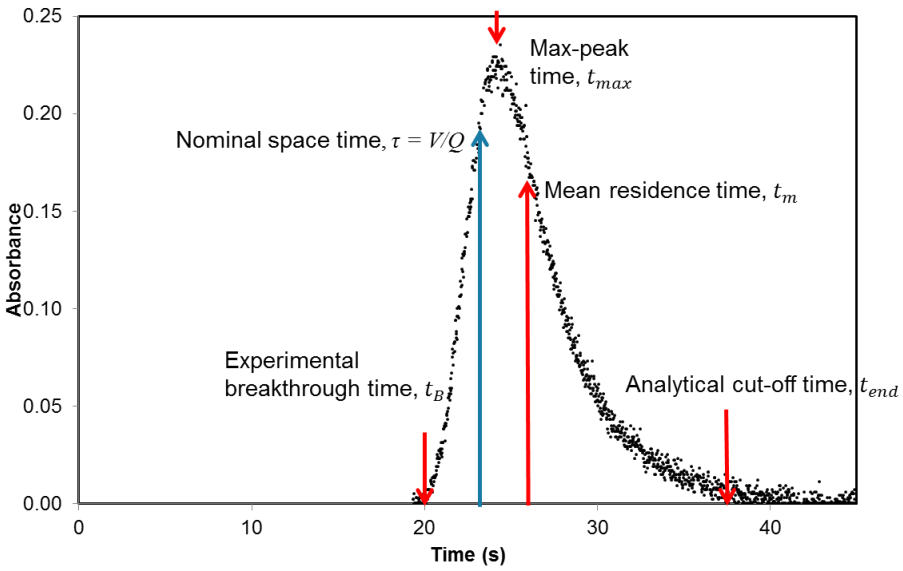

Figure 11 – Time definitions.

The mean residence time is defined according to the exit age distribution E(t) [18].

$$t_m = \int_0^\infty tE(t)dt \tag{5}$$

$$E(t) = \frac{C(t)}{\int_0^\infty C(t)dt} \tag{6}$$

The exit age distribution, by definition gives

$$\int_0^\infty E(t)dt = 1 \tag{7}$$

Dimensionless or normalized values, as defined bellow are used in order to compare RTD curves at different flow rates and in different reactors [18].

$$\theta = \frac{t}{t_m} \tag{8}$$

$$E(\theta) = t_m E(t) \tag{9}$$

Mean residence time is the first moment of an RTD curve [18]. The second and third moment, variance and skewness respectively, are often used to describe RTD curves and are defined as

$$\sigma^2 = \int_0^\infty (t - t_m)^2 E(t) dt \tag{10}$$

$$s^3 = \frac{1}{\sigma^{3/2}} \int_0^\infty (t - t_m)^3 E(t) dt \tag{11}$$

Skewness describes the symmetry of the curve; the skewness of a perfectly symmetrical curve is equal to zero. Skewness can be positive or negative based on which direction the curve is skewed. In RTD curves, curves are typically skewed towards the left due to tailing. The variance describes the spread or width of the curve. Variance can also be expressed as a dimensionless group by dividing by t_m^2. Low variance indicates low axial mixing, and therefore narrow RTD curves. Increased variance is indicative of departure from plug flow pattern.

2.4 Modelling

As mentioned, most works on RTD in micro-reactors have a focus on modelling. In order to properly model an RTD curve, it is necessary to identify the flow pattern. There are two theoretical flow patterns in tubular reactors: laminar and plug/inviscid flow [20]. Multiple models exist for both, and some combination/transition models have also been developed.

2.4.1 Single parameter turbulent models

In an ideal plug flow reactor, a pulse entering the reactor would exit the reactor as the same pulse. In practice, turbulence and diffusion cause axial mixing, distributing the pulse's exit over a wider timespan. A common model which is used to model non-ideal plug flow RTD curves is

the axial dispersion model with open-open boundaries [33] as illustrated by Figure 12 and as defined

$$E(\theta) = \frac{1}{2}\sqrt{\frac{Pe}{\pi\theta}}\, exp\left\{-\frac{Pe(1-\theta)^2}{(4\theta)}\right\} \tag{12}$$

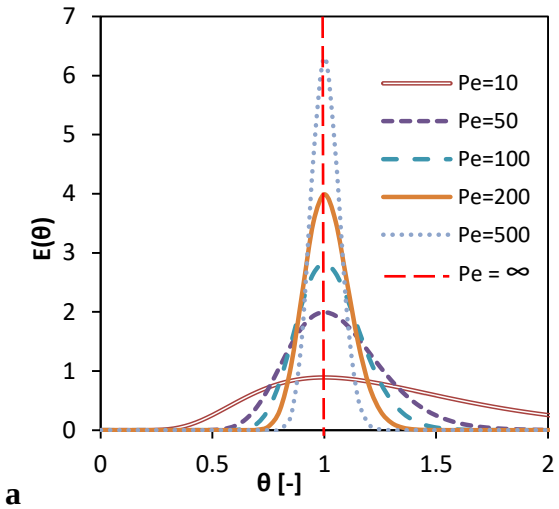

a

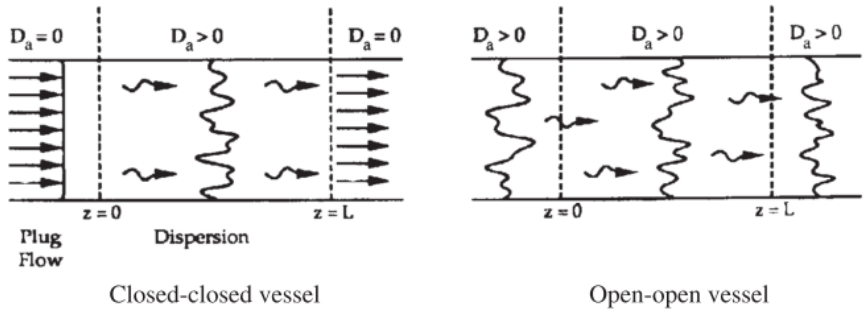

b

Figure 12 – (a) Dispersion model at different Pe and (b) boundary conditions [34]**.**

The dispersion model is often used due to its simplicity, having only one parameter, and to its good fit to near plug-flow RTD curves; the most common problem with this model is the lack of tailing prediction. The open-open condition was chosen because it is the nearest estimation of the actual conditions: dispersion occurs in the tubing prior to and after the reactor. It is estimated

that the boundary conditions assumption becomes less important as the model approaches plug flow (Pe>100), therefore it is not necessary to precisely quantify the dispersion at the boundaries [20].

The Peclet number, Pe,

$$Pe = \frac{uL}{D} = \frac{Mass\ transfer\ due\ to\ convection}{Mass\ transfer\ due\ to\ dispersion} \quad (13)$$

is the dimensionless group which is inversely proportional to the dispersion where the dispersion model applies. An ideal plug flow system, in which no dispersion occurs, has an infinitely high Pe. The lower the Pe, the farther the system deviates from plug flow. As a rule of thumb, a Peclet number above 100 indicates near-plug flow behaviour but the RTD must also be symmetrical for the dispersion model to fit [34].

For this model, Pe can be analytically determined using the experimentally determined dimensionless variance [34]

$$\frac{\sigma^2}{{t_m}^2} = \frac{2Pe_r + 8}{Pe_r^2 + 4Pe_r + 4} \quad (14)$$

Another commonly used model is the tank-in-series model, which models a PFR type reactor as CSTRs in series. This model is very similar to the dispersion model [34] and the two models can be related as

$$\mathrm{N} = \frac{Pe_r}{2} + 1 \quad (15)$$

where N is the number of CSTRs in series. It is therefore not necessary to explore the tank-in-series model independently.

2.4.2 Laminar Models

In an ideal laminar tubular reactor, the fluid travels through the reactor with a parabolic profile where the fluid at the center of the reactor travels at the fastest velocity and exits the reactor at the theoretical breakthrough time [20]

$$t_B = \frac{L}{u_{max}} = \frac{\tau}{2} \tag{16}$$

Note that this is only the case for a straight, circular tube. Martinelli et al. [35] used CFD to work out that for a straight, rectangular tube

$$t_B = \frac{L}{u_{max}} = \frac{\tau}{-0.56\left(\frac{h}{w}\right)^2 + 1.5\left(\frac{h}{w}\right) + 1.5} \tag{17}$$

Furthermore, curved or otherwise obstructed tubular reactors will introduce secondary and potentially chaotic flow, and the RTD will deviate from the ideal curve ($E(\theta) = \frac{1}{2\theta^3}\ when\ \theta > \frac{1}{2}$) shown in Figure 13. Chaotic secondary flow can increase or decrease the breakthrough time, introduce axial mixing, and/or shorten tailing effect.

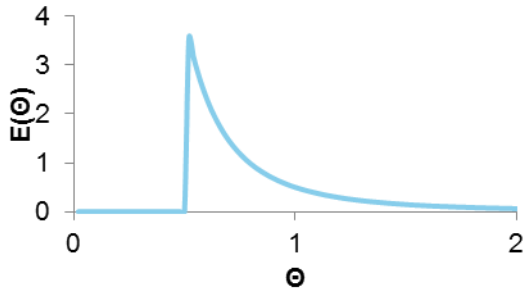

Figure 13 – Ideal laminar model in a tubular reactor [20]**.**

Non-ideal, one-parameter, laminar models which have been developed include [36]:

- the generalized convection model, which has a parameterized breakthrough time of $\alpha\tau$,
- the generalized power-law model, where the breakthrough time is $\left(\frac{n+1}{3n+1}\right)\tau$, and
- the combined PFR+CSTR model, in which the breakthrough time is defined as the mean residence time in the plug-flow region.

2.4.3 Multi-parameter Models

The models described above are single-parameter models, but these are not always a good fit, especially for combination flow patterns which cause non-laminar, asymmetrical RTD curves. To better model these types of curves, multi-parameter models have been developed. The one that will be used in this paper is Ham et al.'s [25] three-parameter, semi-empirical model "Model B" due to the very small difference they found between this model and the experimental data in their experiments. This model uses the empirical breakthrough time and end time to estimate θ_{min} and θ_{max}, and then the parameter N is used to fit the model to the curve.

$$E(\theta) = \frac{8N\theta_k^N}{\theta^{N+1}}\left(\frac{\theta}{\theta_{max}}\right)^{N-1}\left[1 - \frac{\theta_k^N}{\theta^N}\left(\frac{\theta}{\theta_{max}}\right)^N\right]^7 \quad (18)$$

$$\theta_k = \frac{\theta_{min}\theta_{max}}{\theta_{max} - \theta_{min}} \quad (19)$$

Ham et al.'s [25] suggest using a slightly larger θ_{max} and a slightly lower θ_{min} due to the loss of accuracy at the ends of the curve. As was demonstrated previously data is lost on both ends, but especially at the end point due to tailing. They also produced a graph showing the dependence of N on θ_{min} and θ_{max}, which was used at a starting point for iterative curve fitting.

3 Results and Discussion

3.1 Coil Reactors

Coils have been extensively studied because they have a simple geometry which can induce secondary flow. The applicability of the dispersion model and the dependability of Pe on Re depends on Re, on the ratio between the tube and coil diameter, and on the length. The coil reactors studied here where used as a baseline for further experiments. The parameters were chosen to overlap with the residence time and Re generated in the serpentine plate reactors. This gave flow rates between 20 g/min and 100 g/min. The RTD moments are given in Table 2. As seen in Figure 14, at these flow rates, the dispersion model does not fit these RTD curves due to the asymmetry.

Table 2 – Average time t_m, variance σ^2, and skewness s^3 of Teflon coils.

Flowrate (g/min)	Re	De	t_m (s)	σ^2 (s^2)	s^3	σ^2/ t_m^2
Single direction coil						
20	121	31	39.3	154.2	47	0.100
40	241	62	18.8	20.2	9.9	0.057
60	362	93	12.2	4.5	3.9	0.031
100	603	155	8.0	2.3	2.6	0.036
Figure-8 coil						
20	121		40.4	61.8	20	0.038
40	241		20.2	18.9	8.4	0.047
60	362		13.5	4.8	2.9	0.027
100	603		8.6	1.9	1.5	0.025

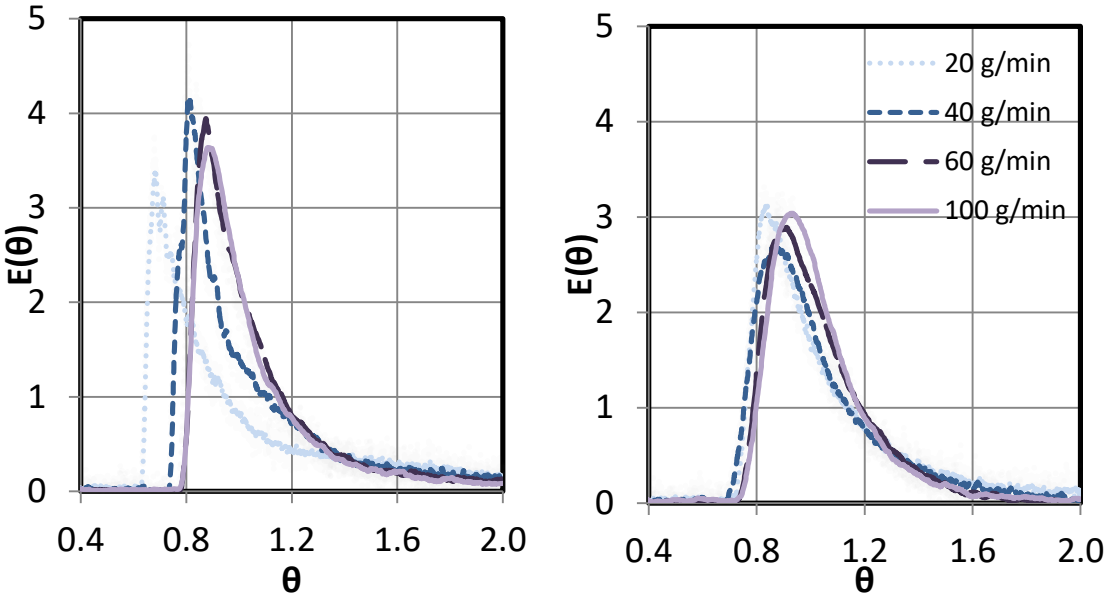

Figure 14 – Single coil (left) and figure-8 coil (right) (1/4") RTD curves.

With the single direction coil, the RTD curve has long thin tailing and is shaped like a laminar model. At 20 g/min (De = 31) the flow is still expected to be unidirectional. At the higher flow rates, the shape is indicating that no strong secondary flow was formed despite the Dean number being above the critical Dean number; this is due to the relatively short length of the reactor. The dispersion model is only applicable "when the pipe is long enough to achieve radial uniformity of a pulse of tracer"; according to Levenspiel "this may require a rather long pipe" [20]. Sharma et al [27] were able to fit the dispersion model with Pe < 100 (not nearing plug flow) to an RTD of a coil of approximately the same curvature ratio and Re as is presented here with a length of 14 meters. Since the tested reactor is of only 1.6 m, it is not surprising that the pulse does not have enough time to disperse more evenly as it did with Sharma et al.'s experiment.

The flow rate had only a slight effect on the RTD curve. Generally, the increased flow rate improves the symmetry of the curve but in this range, the effect is not significant which is in accordance with Trivedi et al.'s findings that the dispersion is necessarily not dependent on the Re in circular tube coils [30].

It has been shown that even a single inversion can reduce the variance of the RTD curve, although at Re<2000, increasing Re may not reduce variance [27]. This may be explained by De becoming less significant when Re is large enough to instill a non-laminar flow regime. The figure-8 coil is a better approximation of the serpentine channel plate reactor due to the inverting curves. In this reactor there is an absence of the thin tailing found in the single coil. While these curves are still too asymmetrical to fit a dispersion model, it also differs significantly from the laminar model; this indicates that secondary flow is occurring. While not attempted here, a multi-parameter would be most appropriate for this reactor.

Since these reactors are of the same volume, they can be compared directly with dimensional curves as shown in Figure 15. From this, the effect of single direction coiling vs inverting coiling is clear: for the same coil and tube diameter, the inverting coiling induces more significant secondary flow. This leads to a narrower and more symmetrical residence time distribution curve.

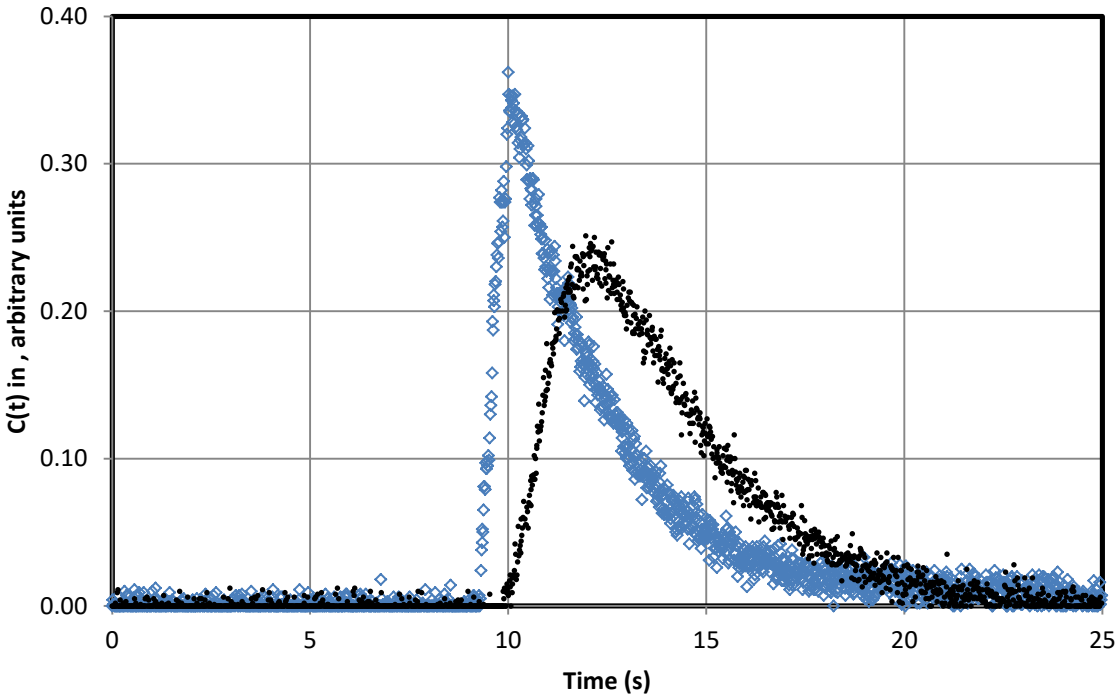

Figure 15 – 1/4" Single coil (empty diamonds) and figure-8 coil (filled circles) sensor response curves at 60 g/min.

While not directly comparable to the plates due to channel shape, the results give an idea of the effect of the alternating curvature direction. As noted previously, conventional wisdom is to have more than one turn on each coil arm and a minimized pitch in order to effectively induce secondary flow. Here it has been shown that a single turn, a geometry which is achievable in a reactor plate, is sufficient to have some effect on the RTD.

3.2 Serpentine Channel Reactor Plates

3.2.1 Without mixing zone

The two serpentine channel plates without mixing zones were studied at flowrates between 35 and 105 g/min. Increasing the volume by increasing the depth of the serpentine plates, while keeping the width constant, decreases the surface to volume ratio and therefore the heat exchange capability of the plate.

The serpentine 0.5 mm plate has an RTD with significant tailing, as seen in Figure 16, but does not appear to be purely laminar. As with the inverted coil, this makes it difficult to model as it is likely to be best fit by a combined model. This does suggest, however, that eddies are being induced by the alternating curves. With a radius of 6 mm, the Dean numbers being generated in the curved sections of the channel are 15-105 at the tested flow rates. As has been previously noted, when De < 40, the flow is still largely unidirectional. At between 40 and 105, vortices are being formed, but the issue is likely that the vortices does not carry through the straight channels, causing laminar flow (i.e., unidirectional) patterns to form. As with the coils, there is no significant difference between the different flow rates which is expected in laminar flow.

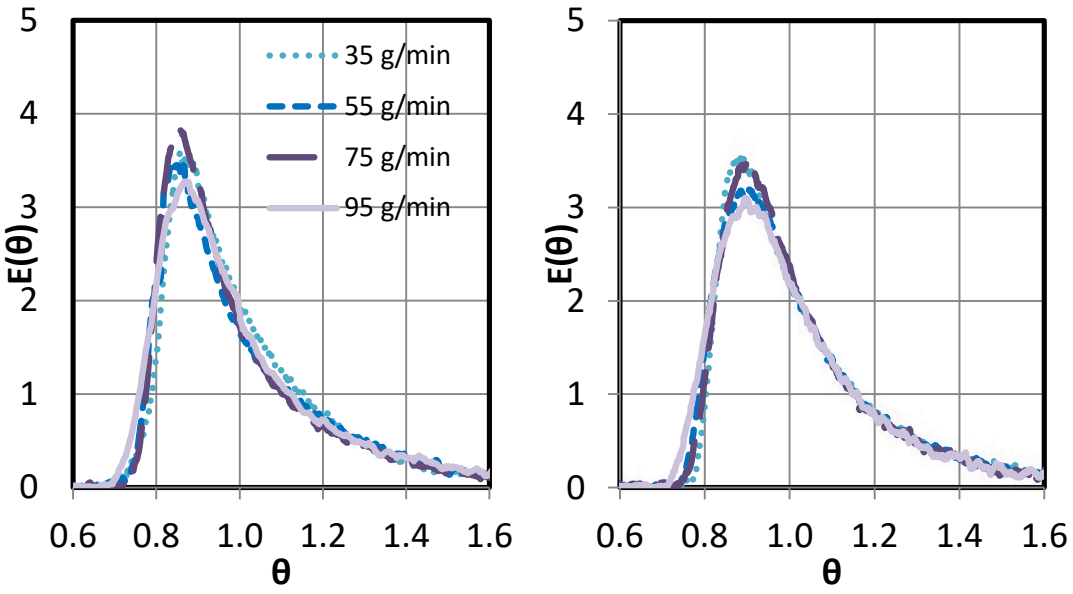

Figure 16 – RTD of serpentine channel plate with depth of 0.5 mm (left) and 1.0 mm (right).

It has been shown that the aspect ratio, depth divided by width, can have an effect on the RTD. Howell et al. demonstrated that deeper curved channels have better radial mixing [37], but most studies focused on aspect ratios around or larger than 1.0. While the depth of one plate is

doubled, going from 0.5 mm to 1.0 mm, the aspect ratio, 0.05 and 0.10 respectively, is well below 1.0 for both plates. This may account for the similarity in the RTD curve for the 1.0 mm depth serpentine plate, as shown in Figure 16.

Both serpentine plates have a larger nominal space time larger than the mean residence time with an error ranging from 6 to 12%. This indicates that there are deadzones in these plates, likely due to the corners of the rectangular channel. However, this difference decreased as the flow rate increased, perhaps because there is slightly better mixing at higher flow rates.

3.2.2 With mixing zone

As mentioned, for single phase systems, it is useful to have initial vigorous mesomixing prior to allowing the reaction medium to reside in a serpentine channel. The plates studied in this section have either SZ or TG mixing zones prior to the serpentine channel. The serpentine plates with TG and SZ mixing zones (mix-then-reside) were designed for single phase flow but can lead to hotspots in the mixing portion where the reaction occurs at the fastest rate [38].

Because the mixing zone is small compared to the total volume, the effect of mixing zone is too small to have a significant effect on the overall RTD; the RTD curves of all the plates studied in this section have the same shape as Figure 16, with significant tailing and a rounded peak. Therefore, while the mesomixing is improved by the addition of a small mixing zone, the overall macromixing flow pattern is not affected, making it more predictable.

The lack of significant effect that the mixing zone has on the RTD of the serpentine plates is even more apparent when evaluating the three moments, as given in

Table 3. When evaluating the plates at the same depth, the dimensionless variance is also given in order to be able to compare between flow rates and at the two different depths.

Table 3 – Average time t_m, variance σ^2, and skewness s^3 of serpentine channel plates with and without mixing zones.

Flowrate (g/min)	Re	De	t_m (s)	σ^2 (s^2)	s^3	σ^2/ t_m^2
No mixing zone (0.5 mm)						
35	125	35	13.8	5.7	4.2	0.030
55	196	55	8.5	2.7	2.6	0.037
75	268	76	6.6	1.6	1.9	0.037
95	339	96	5.2	1.0	1.3	0.037
TG (0.5 mm)						
35			15.1	6.7	4.5	0.029
55			10.3	3.7	3.6	0.035
75			6.9	0.9	1.1	0.019
95			5.1	0.7	0.7	0.027
SZ (0.5 mm)						
35			14.7	6.4	5.1	0.030
55			9.2	2.8	2.9	0.033
75			6.9	1.6	2.1	0.034
95			5.3	1.0	1.4	0.036
No mixing zone (1.0 mm)						
35	119	46	25.1	15.9	9.0	0.025
55	187	73	15.8	6.9	4.3	0.028
75	255	99	13.1	3.8	2.8	0.022
95	323	126	9.0	2.6	2.1	0.032
TG (1.0 mm)						
35			25.8	11.7	4.4	0.018
55			15.9	5.0	2.6	0.020
75			12.3	4.1	2.4	0.027
95			9.7	2.9	1.6	0.031
SZ (1.0 mm)						
35			25.9	11.6	6.5	0.017
55			16.6	5.2	3.6	0.019
75			11.8	3.4	3.2	0.024
95			9.4	2.0	1.6	0.023

As with the serpentine plates and as evidenced by the dimensionless variance, there is no clear dependence on the flow rate. Due to the lack of difference between the plates with and without the mixing zones, it is also not apparent from these experiments which mixer geometry, between the TG and SZ, has the better macromixing. However, the mesomixing performance primarily scales with energy dissipation rate when the mixers induce chaotic eddies at high Re [39].

3.3 Liquid-Liquid Reactor Plates

The LL plate micro-reactor with continuous mixers has been shown to have effective mesomixing for fast liquid-liquid reactions [40]. The continuous mixers are akin to multiple CSTRs in series; As discussed previously, CSTRs in series can be modeled with symmetrical RTD curves similar to the dispersion model. It is therefore expected that the RTD for this plate have a good fit with the dispersion model. The best fit was determined by maximizing the R^2 which is calculated as follows:

$$SS_{res} = \sum (y_i - f_i)^2 \tag{20}$$

$$SS_{tot} = \sum (y_i - \bar{y})^2 \tag{21}$$

$$\bar{y} = \frac{1}{n}\sum y_i \tag{22}$$

$$R^2 = 1 - \frac{SS_{res}}{SS_{tot}} \tag{23}$$

The RTD curves and the best-fit model curves for this plate are shown in Figure 17. While the LL plate RTD curves are still slightly off-centre due to back-end tailing, the curves are fairly symmetrical. Both the symmetry and narrowness, and therefore the model fit, increases with increasing flowrate. The R^2 at 15 g/min was 0.905 and the R^2 at 55 g/min was 0.944.

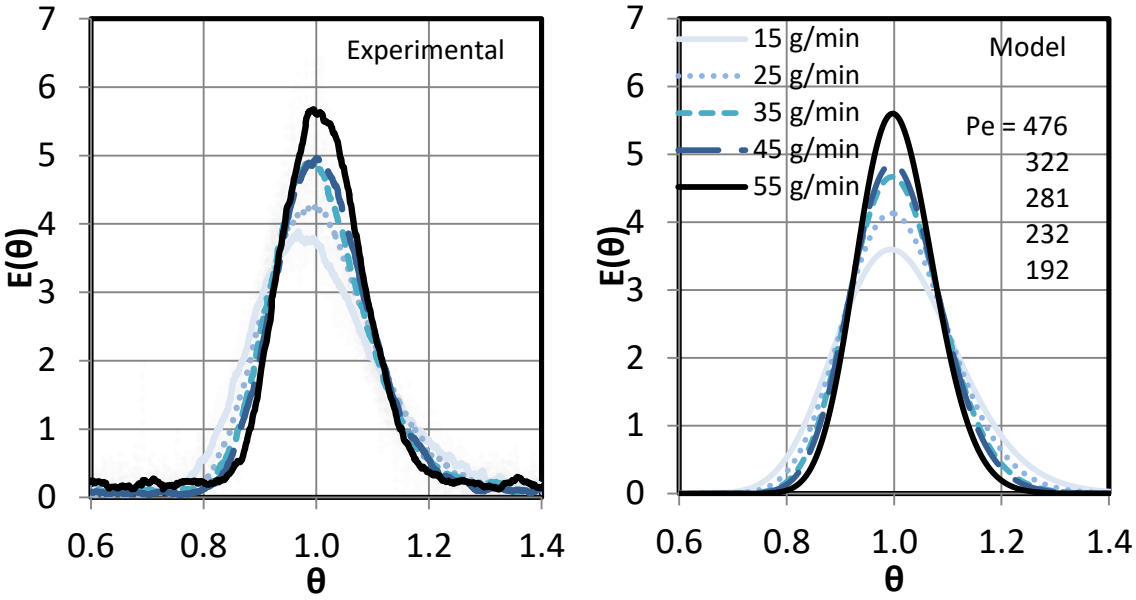

Figure 17 – RTD of LL continuous mixing plate (left) and model RTD curves (right).

3.3.1 Effect of Micro-Mixer Spacing

The different interspacing arrangements were characterized, allowing to the optimization of the geometrical design. By adding straight channels between mixers, the volume, and therefore residence time, is increased while the energy consumption (i.e. pressure drop) is decreased. However, having fewer mixers can affect the rate of mass transfer in a liquid-liquid system and can affect the RTD. To aid in determining the optimal arrangement, the effect of spacing on macromixing is presented here. The grouped and minimal mixers are placed directly after the curves because phase separation can occur due to centrifugal forces [38]. The RTD moments for all four spacing arrangements are presented in Table 4.

Table 4 – Average time t_m, variance σ^2, and skewness s^3 of LL reactor plates.

Flowrate (g/min)	Re	t_m (s)	σ^2 (s^2)	s^3	σ^2 / t_m^2
Continuous					
15	321	43.9	20.7	2.7	0.011
35	749	20.9	3.2	0.86	0.007
55	1177	13.1	0.72	0.17	0.004
Equally spaced					
15	321	74.9	97.0	13.1	0.017
35	749	35.2	13.9	3.95	0.011
55	1177	22.7	3.59	1.65	0.007
75	1605	16.5	1.47	0.70	0.005
95	2033	13.2	0.89	0.51	0.005
Grouped					
15	321	77.8	97.1	14.7	0.016
35	749	36.0	17.9	5.91	0.014
55	1177	23.3	6.58	3.27	0.012
75	1605	17.3	3.52	2.46	0.012
95	2033	14.3	2.07	1.66	0.010
Minimal					
15	321	79.1	189.2	38.9	0.030
35	749	38.0	25.3	9.8	0.018
55	1177	25.0	9.33	5.9	0.015
75	1605	17.1	5.19	3.4	0.000
95	2033	15.2	2.85	2.1	0.012

Figure 18 shows the RTD curves of the plate with the equally spaced mixer arrangement. Similarly to the plate with continuous mixing, the RTD narrows and becomes more symmetrical as the flow rate is increased. For this plate, the R^2 at 15 g/min was 0.8804 and the R^2 at 95 g/min was 0.9250. The fit is therefore not as good as the continuous plate, but still has a good fit with the dispersion model.

As mentioned, the criterion for the applicability of the dispersion model is a Pe > 100, which indicates near-plug flow behaviour. As illustrated by Figure 19, this criterion is met at 15

g/min for both plates, with Pe increasing as flowrate increases. This behaviour is consistent with turbulent flow in straight tubes although the Re number is not yet in the turbulent regime.

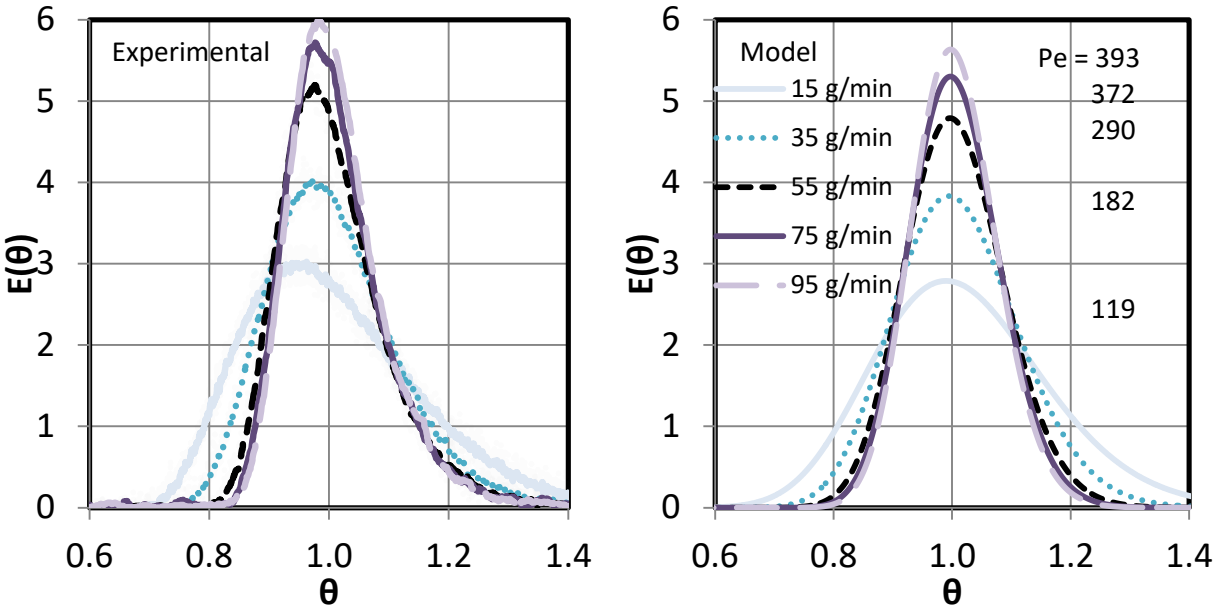

Figure 18 – RTD of LL plate (equally spaced) and model RTD curves.

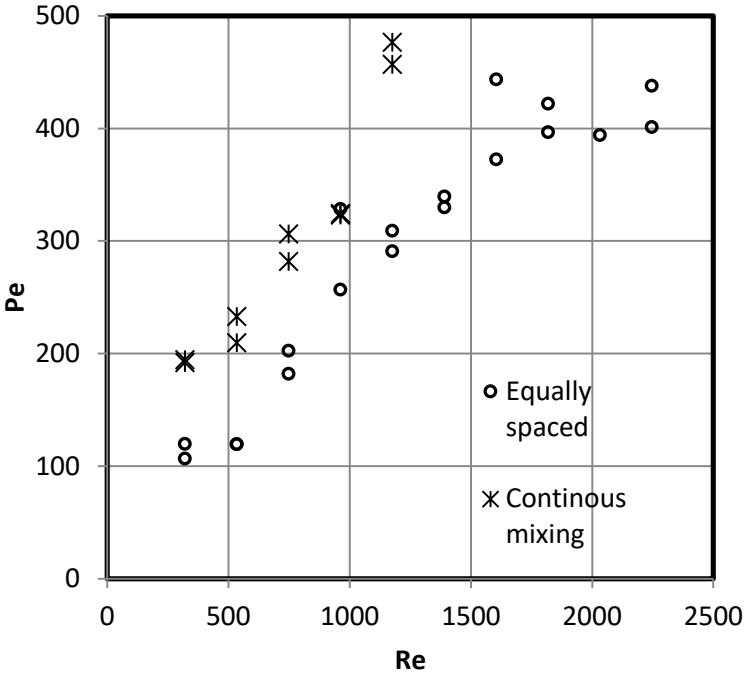

Figure 19 – Pe vs Re for LL plates (continuous and equally spaced mixers)

When the dispersion model applies, Pe is often correlated to Re using a power law. In the laminar regime, Pe is a function of Re and Sc in a straight, circular tube. In the turbulent regime, no theoretical correlation exists, but a range of experimental results have been modeled using the power law. [41] The best fit power law for the experimental data for these two plates are:

$Pe = 4.4\ Re^{0.63}$ $R^2 = 0.89$ (Continuous) (24)

$Pe = 1.1\ Re^{0.79}$ $R^2 = 0.92$ (equally spaced) (25)

While the Pe is higher of the continuous mixing plate, this plate had a greater disparity between t_m and τ, with an error of -1 to -18%, typically with the error increasing with flow rate. The error for the equally spaced mixer plate ranged from +5% at 15 g/min to -5% at 95 g/min. This is likely due to some recirculation occurring at higher flowrates. As a result, the axial dispersion increases with flowrate. The axial dispersion, which is seven to eight orders of magnitude larger than the diffusivity of fluorescein salt, was calculated from the Peclet number as is presented in Figure 20.

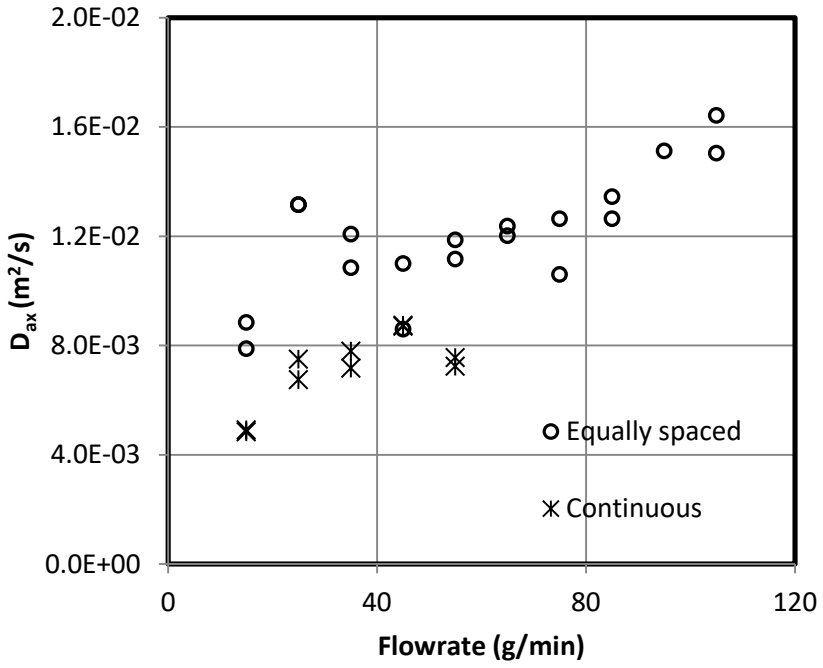

Figure 20 – D_{ax} vs flowrate for LL plates (continuous and equally spaced mixers)

The plate with the grouped mixers has the same number of mixers as the plate with the equally spaced mixers, therefore have similar average energy dissipation rate (mesomixing) at a particular flow rate. However, the increased length of the straight segment increases the asymmetry or the RTD, shown in Figure 21.

The tailing effect is even more pronounced in the RTD of the LL plate with minimal mixers and grouped mixers, shown in the same figure. This is likely due to laminar flow (unidirectional) patterns starting to form in the straight channels [42]. The Re in the straight channel ranges from 85 to 540 which placing it in the laminar regime. The length needed fully form laminar flow in these straight channels, known as the entrance length, can be estimated by $0.06*d_t*Re$ [42]. It would therefore require channel lengths greater than 14.5 mm at the lowest Re and 77 mm at the highest. Laminar flow therefore fully develops in the straight channels of

both plates where the straight channel length is 82 mm and 91 mm for the grouped and minimally spaced mixing plates, respectively. The equally spaced mixers have a straight channel of 32 mm between them; therefore laminar flow would only fully develop at flowrates below 30 g/min. Like in the continuous mixer and equally spaced mixer plates, increasing the flow rate increases symmetry and narrows the curve. However, the skewness in both plates at these flow rates results in the dispersion model not being an appropriate model.

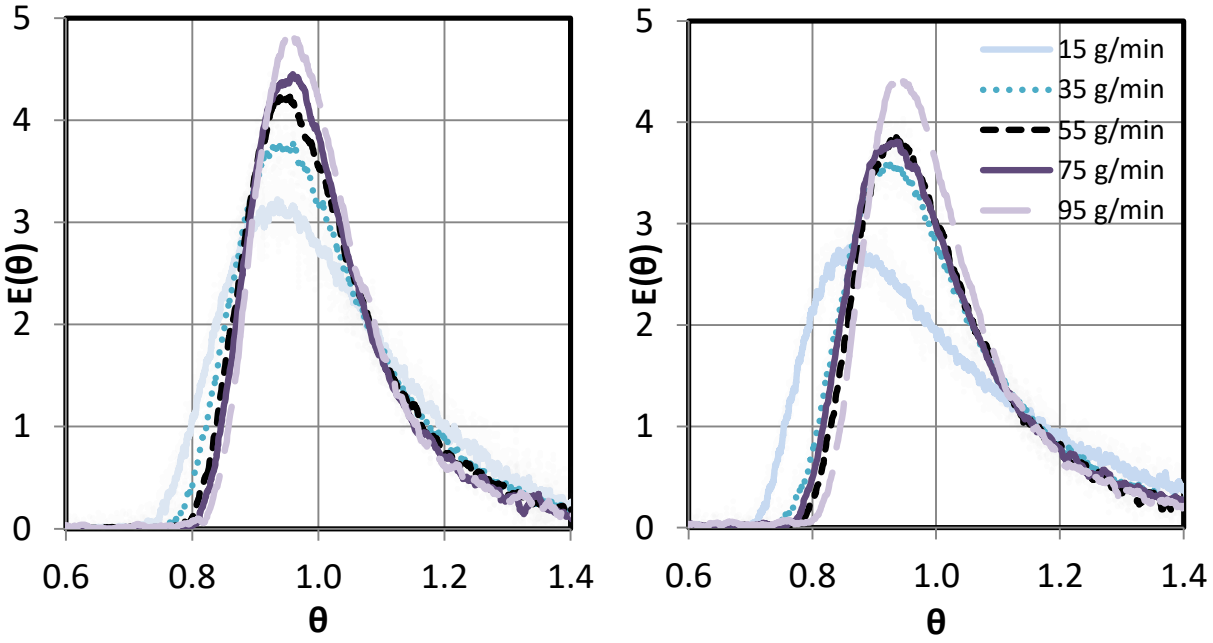

Figure 21 – RTD curves at various flow rates in LL plates with grouped mixers (left) and minimal mixers (right).

Since the dispersion model is not appropriate for these plates, Ham et al.'s semi-empiric, three parameter model was used to model the curves as demonstrated in Figure 22. For all the curves, the empirical model is a close fit for the off-centre peak of the curve and an acceptable fit for the tail although. The parameter values and R^2 are presented in Table 5. While the parameters can be adjusted to better fit the tail, the resulting parameters are less true to the breakthrough and

end times. Although not perfectly analogous, and therefore not mathematically derivable from the model, the increase of parameter N in this model correlates to an increase in the Peclet number. This can be visually confirmed by the increased symmetry as the flow rate increases, along with an increase in the parameter N. However, since the dispersion model is a poor fit, it can be inferred that Pe < 100 for these plates in this range of flowrates. As a point of comparison, the same model was fit to the equally spaced mixer plate and the continuous mixing plate, both of which fit the dispersion model. The parameters for these are in Table 6. Similarly, the N parameter increases as flowrate increases and the difference between the min and max times narrows.

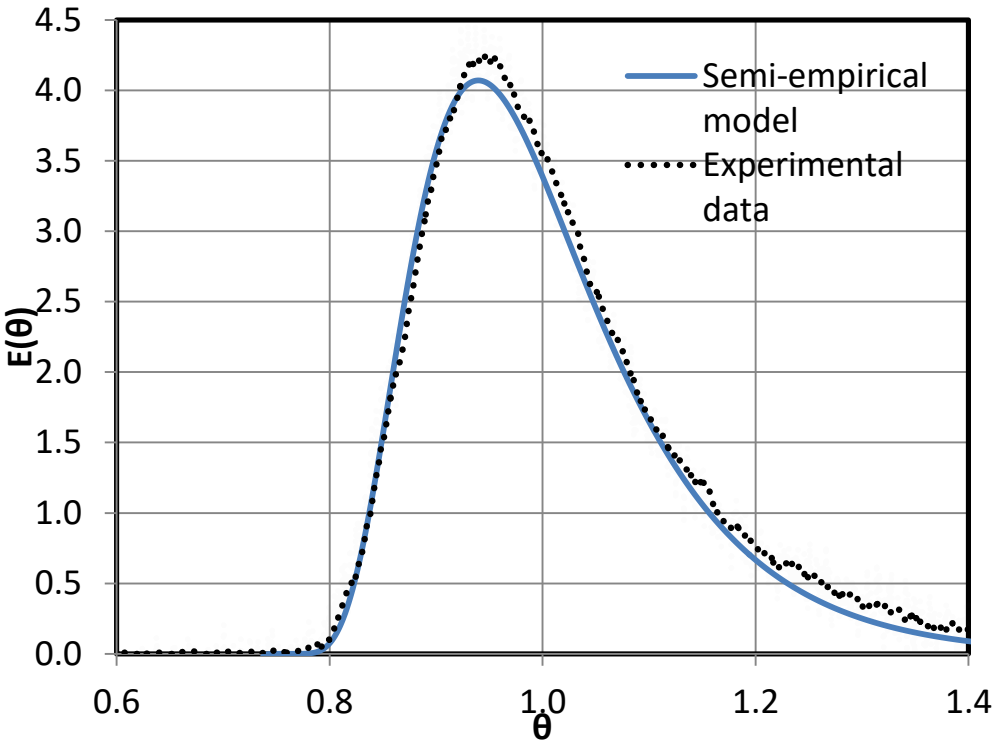

Figure 22 – Semi-empirical model fit to the RTD of the LL plate with minimal mixers at 55 g/min.

Table 5 – Semi-empirical model parameters for LL plates with grouped and minimal mixers

Flowrate (g/min)	Spacing	θ_{min}	θ_{max}	N	R^2
15	Grouped	0.62	1.60	3.54	0.9500
	Minimal	0.52	1.95	4.23	0.9176
35	Grouped	0.66	1.95	3.71	0.9724
	Minimal	0.64	1.78	4.57	0.9768
55	Grouped	0.69	1.51	4.05	0.9762
	Minimal	0.66	1.75	4.76	0.9822
75	Grouped	0.71	1.50	4.18	0.9763
	Minimal	0.66	1.75	4.90	0.9787
95	Grouped	0.73	1.47	4.42	0.9793
	Minimal	0.67	1.75	5.28	0.9795

Table 6 – Semi-empirical model parameters for LL plates with continuous and equally spaced mixers

Flowrate (g/min)	Spacing	θ_{min}	θ_{max}	N	R^2
15	Equal	0.62	1.50	3.06	0.9697
	Continuous	0.68	1.35	2.96	0.9571
35	Equal	0.72	1.36	3.27	0.9712
	Continuous	0.76	1.25	2.96	0.9730
55	Equal	0.75	1.37	4.08	0.9912
	Continuous	0.77	1.21	2.91	0.9476
75	Equal	0.73	1.23	4.02	0.9772
95	Equal	0.74	1.46	5.27	0.9854

3.4 Comparison of the geometries.

In general, as turbulence is increased, the RTD narrows. An increased in energy dissipation benefits both the macroscopic features of plug flow and microscopic features of mixing [38]; naturally at the expense of pressure drop, and thereby greater pump power.

For this reason, although they have similar volumes, the LL plates have a much narrower and more symmetrical residence time distribution than the serpentine plate of 1.0 mm depth. In

fact, the serpentine plate is very similar to a figure-8 inverting coil of the same length and approximate volume as seen in Figure 23. Furthermore, for similar residence times, the LL plate with equally spaced mixers has the advantage of a more desirable RTD over the LL plate with minimal mixers, within the LL plate's operating range of flowrates. It can also be seen graphically in Figure 23 that the equally spaced plate has a Pe much greater than 100.

At the low Reynold numbers (40-350) studied here, the serpentine plates do not achieve near-plug flow conditions unlike other commercial complex micro-reactors (LTF, Chemtrix, etc.) with much smaller channel dimensions at similar Re [43], [44]. Coil flow inverters of similar size did achieve near-plug flow at higher Re (Re > 8000; De > 3000) [27], which indicates that the serpentine plates may be more competitive at higher flow rates.

As noted previously, the disparity between the mean residence time and the nominal residence time indicates some recirculation, especially as flow rate increased. This is not, however, reflected in the RTD curve. Nieves-Remacha et al studied a continuous mixing reactor plate with heart-shaped mixers at flow rates between 20 and 80 mL/min. Recirculation and dead-zones were noted visually. This was also reflected in the RTD measures: Pe decreased with increasing flow rates and mid-range flow rates caused asymmetrical RTD curves. [24] Since this was not the case with the equally spaced and continuous LL plates, it can be surmised that the recirculation is not as severe.

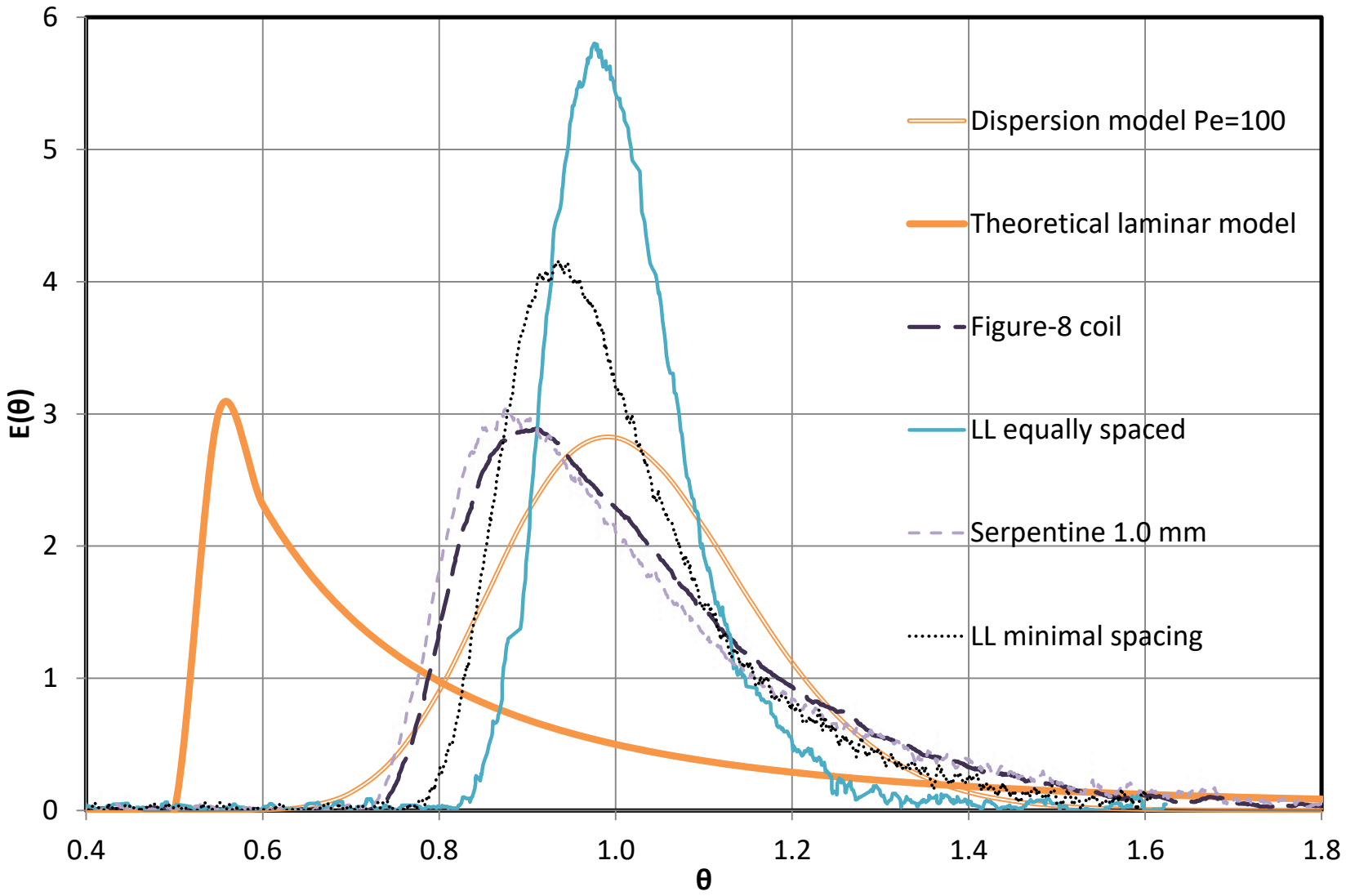

Figure 23 – Comparison of RTDs of geometries at 60 g/min.

4 Implications: Nanoparticle Crystallization in Micro-reactors

4.1 Background

In industry, large scale production of fine particles is typically done in batch reactors. This method can have a negative impact of the performance of the particles. This is due to the difficulties surrounding the control of the product's key characteristics: size, size distribution, and shape. [45] In a batch reactor there is a high variability of the energy dissipation rate where close to the stirrer it is rather high while on the edge almost absent [15]. These properties can be more precisely controlled in a micro-reactor as there is a greater control of mixing, temperature, nucleation, and diffusion [45].

Also of interest is the control of RTD and a quite more evenly distributed energy dissipation rate which is provided by micro-reactors. It has been demonstrated and discussed previously that the liquid-liquid reactor is near plug-flow, and provides constant mixing. Each particle therefore has about the same growth rate and time within the reactor.

It was reported that Nieves-Remacha et al. used a polystyrene precipitation reaction in the micro-reactor with continuous heart-shaped mixers and it outperformed other micro-channel geometries designed for fine particles in terms of particle size [24]. They confirmed that particle size distribution narrowed with higher mixing. It should be noted that this result was repeated in multiple studies [46]. One suggested explanation for this observation is that the shear force breaks up and shapes the particles [47]. Since higher mixing was linked to higher flow rates, another contributory factor may be that the RTD narrowed at higher flow rates. Most of these studies took place in the laminar flow and transient flow regimes.

When dealing with small channels, the risk of plugging caused by particle aggregation must be taken into consideration [48]. Narrow size distribution and the lack of large particle aggregates helps avoid plugging. Strategies that have been used to help avoid plugging in micro-reactors include ultrasonic systems, buffer fluid flow to avoid direct contact with the wall, and periodic purges [45], [48], [49]. Micro-reactor designs that promote narrow size distribution and limit the formation of aggregates allow for a simpler system.

Therefore, when evaluating the suitability of a micro-reactor design for the formation of solid micro- and nano-particles, it must first be determined if the reactor is capable of stable production and secondly if the reactor design increases the control of the key particle characteristics.

4.2 Experimental

An LL plate with continuous mixing, similar to the one previously discussed, was used in this experiment. This plate is near size A7, has fewer mixing elements, and has a glass face as shown in Figure 24. The removable glass face allows the viewing of the process, and also ensures that the plate is easy to clean if plugging occurs.

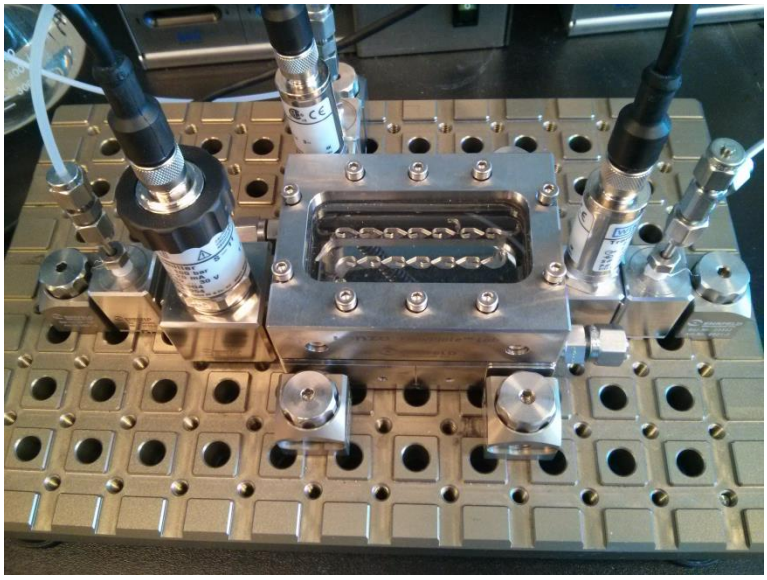

Figure 24 – experimental setup for crystallization reaction with LL plate.

The RTD of this plate in particular could not be determined because the inlet and outlet contribute to a significant portion of the volume and dispersion of the total system but since the mixers are identical, though fewer, to the A5 plate, it is expected that the plate offers a near-plug flow RTD. It was determined that the system as a whole is near-plug flow [50].

The test reaction was the crystallization of silver chloride from silver nitrate (0.05 M) and sodium chloride (0.1 M). Sodium chloride is in excess in order to promote the complete reaction of the silver nitrate. This reaction is fast and silver chloride particles form easily in aqueous solution at room temperature [45].

This is a type A reaction:

$$AgNO_3 + NaCl \rightarrow AgCl\,(s) + Na^+ + NO_3^-$$

Both reactants were fed into the plate with Syrdos syringe pumps at the same flow rate. The reactants met at the first contraction inside the LL micro-mixer. Pressure gauges were placed

at both inlets and at the outlet of the reactor to monitor blockage. Blockage was also visually assessed through the glass panel.

Samples of the outlet mixture were taken, diluted and immediately analyzed using a Malvern ZetaSizer. This provided a number particle size distribution. Multiple measurements were taken to confirm data.

4.3 Results and Discussion

The experiment was performed at 15 and 60 mL/min for 10 minutes each, at which time the pressure increased sharply, forcing the system to stop. As common in micro-reactors when dealing with solids, blockage of the channel occurred over time, as shown in Figure 26.

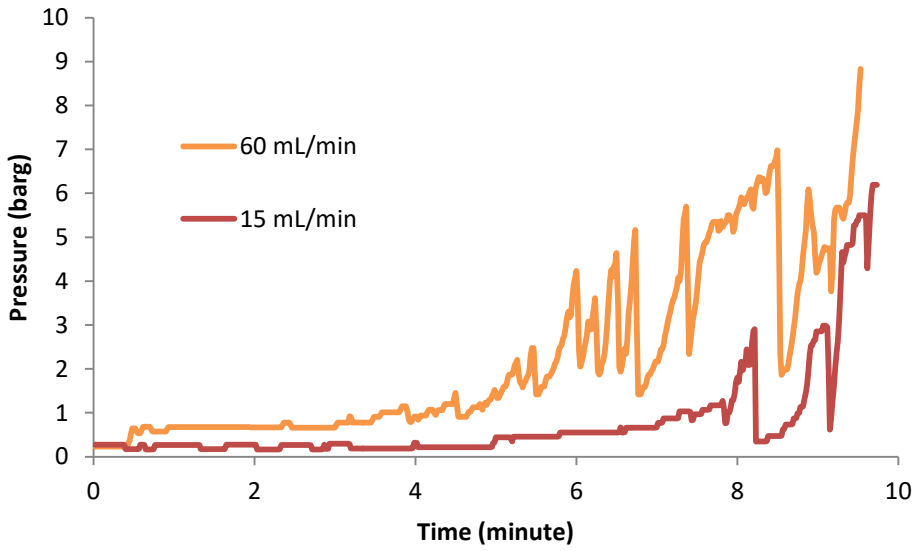

Figure 25 – Inlet pressure during crystallization experiments at 15 and 60 mL/min.

Though the pressure differential was higher at 60 mL/min than at 15 mL/min, the pressure increase follows very similar patterns at both flow rates. From 0 to 5 minutes, the pressure increase is very slight. From 5 minutes to nearly 10 minutes, the pressure increase is much

sharper with a few quick drops when chunks of the accumulating particles broke away. Just short of the 10 minute mark, the experiment had to be stopped due to a sharp increase in pressure, nearing the maximum allowable pressure for the system.

The plugging was most severe in the first two micro-mixers between the contraction and the obstacle as shown in Figure 26. There was also build-up on the walls of the mixer. Because the concentrations of the reactant were already fairly low, it was determined that this reactor is not suitable for precipitation reactions.

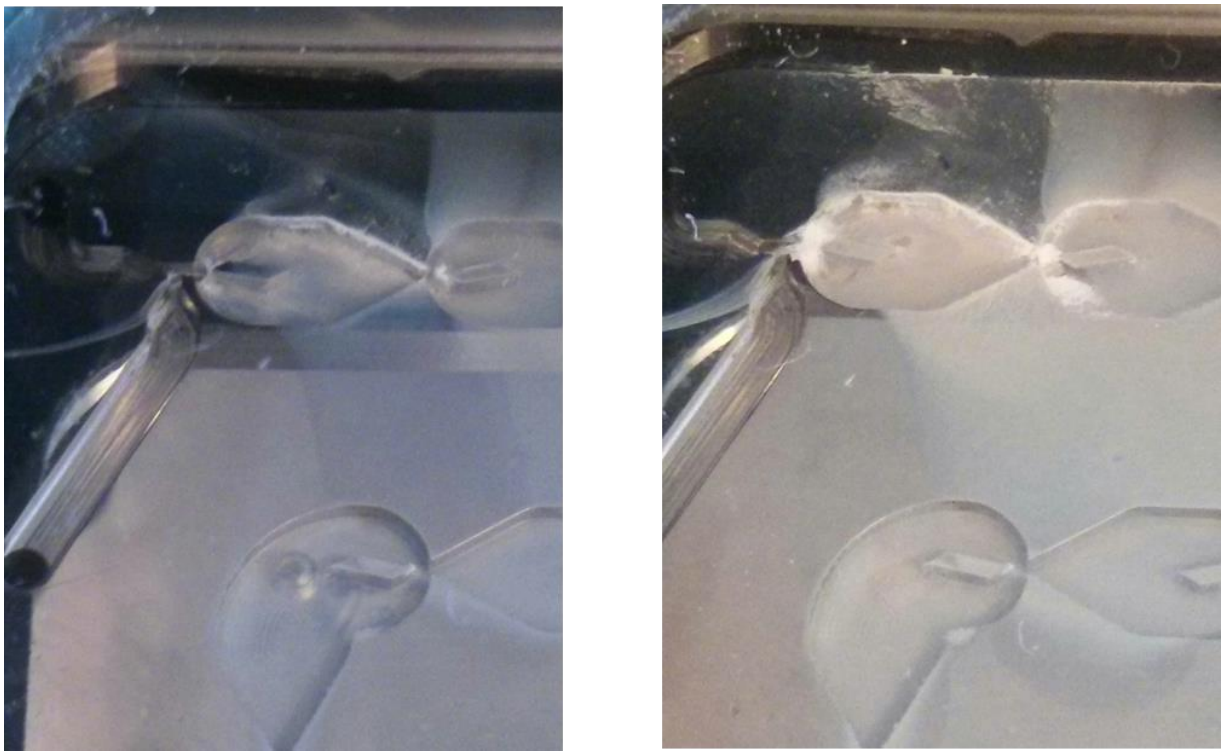

Figure 26 – Plugging at reactor entrance at 60 mL/min at 1 minute (left) and 8 minutes (right).

At the 5 minute mark, samples were taken and the size distribution was determined. Similarly to literature, faster flow rates decreased the particle size and narrowed the particle size distribution as shown in Figure 27. This is likely due to a combination of shorter residence time,

narrower size distribution, and more shear stress on the particles at higher flow rates. The average particle size at 60 mL/min was also much lower (≈69nm) than at 15 mL/min flowrates (≈112nm), consistent with Nagasawa and Mae, who achieved an average particle diameter of 75 nm at 15 mL/min and 50 nm at 50 mL/min in a thin annular stream [45].

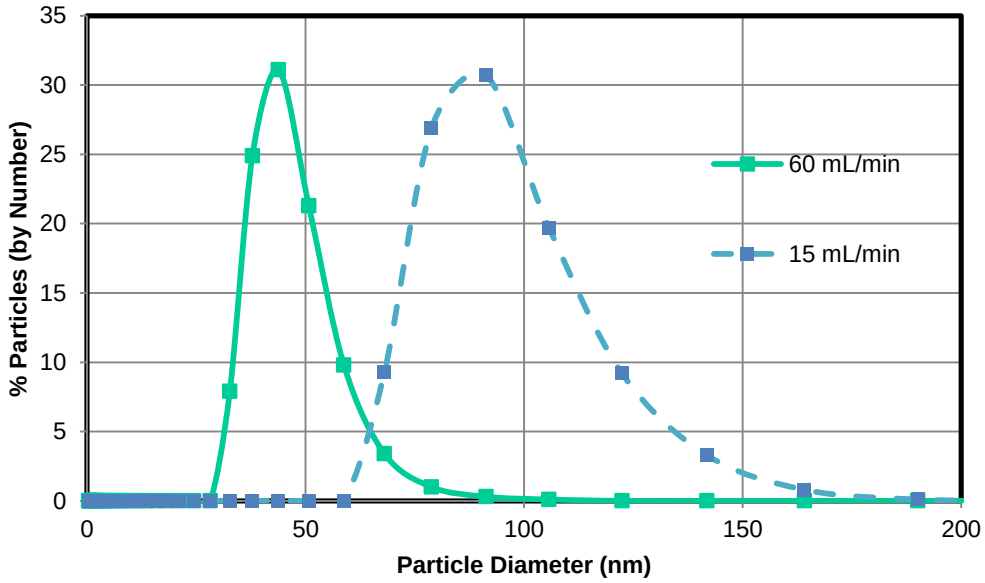

Figure 27 – Particle size distribution in size 300 A7 LL plate after 5 minutes of runtime.

The shape of the PSD curve is similar to the RTD curve with a fairly symmetrical curve and a little tailing. The tailing on the PSD curve is more prominent at the lower flow rate, similarly to the RTD curves.

5 Conclusions and Future Work

5.1 Conclusions

Plouffe et al.'s toolbox approach [17] was expanded upon, evaluating the RTD of commercial micro-reactor plates at flow rates between 15 and 105 g/min. This allows for residence times between 11 seconds and 123 seconds in the A5 plates. In this range near plug-

flow was achieved in two plates: LL with continuous mixers and LL with equally spaced mixers. The dispersion model was fit to the experimental curves at various flow rate for these plates. The applicability criterion was also met with Pe > 100. The correlation between Pe and Re was established for both plates. The Pe was higher and the dispersion model fit was better for the LL plate with continuous mixing than with equally spaced mixers. However, the residence time is longer with the spacing because the straight channels have a greater volume than the mixers. Thus, the LL plate with equally spaced mixers is a good compromise between longer available residence time/volume and narrow, symmetrical residence time distribution.

The plates with grouped and minimal mixers did not fit the dispersion model but the RTD was affected by flow rate and the curves were modeled using a semi-empirical, multi-parameter model. The increased tailing does not make these layouts as attractive as the plate with equally spaced mixers. This results is in contrast with Mielke at al. for the liquid-liquid hydrolysis reaction where the equally-spaced and grouped mixers were shown as being equivalent in the drop flow regime [38].

Serpentine plates with and without mixing zones were characterized. It was determined that the mixing zone at the beginning of the reactor has no significant effect on the overall RTD. These plates have similar RTD curves to an inverting coil. Other works have shown that inverting coils achieve Pe > 100 depending on the Re and tube to coil diameter ratio. It is therefore possible that the plate can achieve Pe >100 at higher Re than tested here.

Finally, the LL micro-reactor plate is not suitable for precipitation reactions due to severe blockage of the channels, causing pressure increase, but the size distribution was narrowed by increased flowrate, as observed in other studies.

5.2 Future Work

Based on the work done here, the following is suggested for future work with these commercial reactors:

- Repeat experiment with LL reactor with triangle obstacle.
- Determine the RTD of the serpentine plates for the full design flowrate range of 35-300 mL/min.
- Expand research on LL reactors RTD to include gas-liquid and liquid-liquid systems.
- Evaluate effect of spacing between micro-mixers on mesomixing.

While micro-reactor plates may not be best suited for precipitation reactions, these are more likely to be successful in an oscillating-flow coil [51]. As a pre-curser to this, the determination of the RTD of such systems is suggested.

6 References

[1] J. Ehgartner, P. Sulzer, T. Burger, A. Kasjanow, D. Bouwes, U. Krühne, I. Klimant, and T. Mayr, "Sensors and Actuators B : Chemical Online analysis of oxygen inside silicon-glass microreactors with integrated optical sensors," *Sensors Actuators B. Chem.*, vol. 228, pp. 748–757, 2016.

[2] Q. Deng, Q. Lei, R. Shen, C. Chen, and L. Zhang, "The continuous kilogram-scale process for the synthesis of 2,4,5-trifluorobromobenzene via Gattermann reaction using microreactors," *Chem. Eng. J.*, vol. 313, pp. 1577–1582, 2017.

[3] L. Vaccaro, "Sustainable Flow Chemistry: Methods and Applications." John Wiley & Sons, Weinheim, p. 336, 2017.

[4] I. Rossetti and M. Compagnoni, "Chemical reaction engineering, process design and scale-up issues at the frontier of synthesis: Flow chemistry," *Chem. Eng. J.*, vol. 296, pp. 56–70, 2016.

[5] A. Paschetag, M. Wesche, H. Nieder, and S. Scholl, "Integration of Ecological Aspects during Process Development and Design - A Case Study of Batch to Continuous Production," *Procedia CIRP*, vol. 48, pp. 532–537, 2016.

[6] S. L. Lee, T. F. O'Connor, X. Yang, C. N. Cruz, S. Chatterjee, R. D. Madurawe, C. M. V Moore, L. X. Yu, and J. Woodcock, "Modernizing Pharmaceutical Manufacturing: from Batch to Continuous Production," *J. Pharm. Innov.*, vol. 10, no. 3, pp. 191–199, 2015.

[7] P. Plouffe, M. Bittel, J. Sieber, D. M. Roberge, and A. Macchi, "On the scale-up of micro-reactors for liquid-liquid reactions," *Chem. Eng. Sci.*, vol. 143, pp. 216–225, 2016.

[8] Y. Su, K. Kuijpers, V. Hessel, and T. Noël, "A convenient numbering-up strategy for the scale-up of gas–liquid photoredox catalysis in flow," *React. Chem. Eng.*, vol. 1, no. 1, pp. 73–81, 2016.

[9] S. Schwolow, J. Y. Ko, N. Kockmann, and T. Reder, "Enhanced heat transfer by exothermic reactions in laminar flow capillary reactors," *Chem. Eng. Sci.*, vol. 141, pp. 356–362, 2016.

[10] E. Mielke, P. Plouffe, N. Koushik, M. Eyholzer, M. Gottsponer, N. Kockmann, A. Macchi, and D. M. Roberge, "Local and overall heat transfer of exothermic reactions in microreactor systems," *React. Chem. Eng.*, vol. 2, pp. 763–775, 2017.

[11] V. Hessel, H. Löwe, and F. Schönfeld, "Micromixers - A review on passive and active mixing principles," *Chem. Eng. Sci.*, vol. 60, no. 8–9 SPEC. ISS., pp. 2479–2501, 2005.

[12] P. Plouffe, D. M. Roberge, and A. Macchi, "Liquid-liquid flow regimes and mass transfer in various micro-reactors," *Chem. Eng. J.*, vol. 300, pp. 9–19, 2016.

[13] D. Bothe, A. Lojewski, and H. Warnecke, "Computational Analysis of Reactive Mixing in

T-Microreactors," in *Micro and Macro Mixing*, 2010, pp. 265–286.

[14] P. Trambouze and J.-P. Euzen, *Chemical Reactors*. Paris: Editions TECHNIP, 2004.

[15] A. Cybulski, J. A. Moulijn, M. M. Sharma, and R.A. Sheldon, "Process Development," in *Fine Chemical Manufacture*, Amsterdam: Elsevier, 2010, pp. 193–413.

[16] S. G. Kandlikar, *Heat transfer and fluid flow in minichannels and microchannels*. Elsevier, 2006.

[17] P. Plouffe, A. Macchi, and D. M. Roberge, "From Batch to Continuous Chemical Synthesis—A Toolbox Approach," *Org. Process Res. Dev.*, pp. 1286–1294, 2014.

[18] H. S. Fogler, "Chapter 13 Distributions of residence times for chemical reactors," in *Elements of Chemical Reaction Engineering*, Fourth Edi., Pearson Education, Inc., 2006, pp. 867–944.

[19] B. T. Kuan, D. R. Lester, W. Yang, and G. Metcalfe, "Chaotic Mixing in a Twisted Pipe : Optimisation of Heat , Mass Transfer and RTD," in *19th Australasian Fluid Mechanics Conference*, 2014, no. December, pp. 5–8.

[20] O. Levenspiel, *Chemical reaction engineering*, vol. 38. 1999.

[21] D. Bošković and S. Loebbecke, "Modelling of the residence time distribution in micromixers," *Chem. Eng. J.*, vol. 135, pp. 138–146, 2007.

[22] E. Georget, J. L. Sauvageat, A. Burbidge, and A. Mathys, "Residence time distributions in a modular micro reaction system," *J. Food Eng.*, vol. 116, no. 4, pp. 910–919, 2013.

[23] S. K. Kurt, M. G. Gelhausen, and N. Kockmann, "Axial Dispersion and Heat Transfer in a Milli/Microstructured Coiled Flow Inverter for Narrow Residence Time Distribution at Laminar Flow," *Chem. Eng. Technol.*, vol. 38, no. 7, pp. 1122–1130, 2015.

[24] M. J. Nieves-Remacha, L. Yang, and K. F. Jensen, "OpenFOAM Computational Fluid Dynamic Simulations of Two-Phase Flow and Mass Transfer in an Advanced-Flow Reactor," *Ind. Eng. Chem. Res.*, vol. 54, pp. 6649–6659, 2015.

[25] J.-H. Ham and B. Platzer, "Semi-Empirical Equations for the Residence Time Distributions in Disperse Systems - Part 1: Continuous Phase," *Chem. Eng. Technol.*, vol. 27, no. 11, pp. 1172–1178, 2004.

[26] T. Casalini, M. Salvalaglio, G. Perale, M. Masi, and C. Cavallotti, "Diffusion and aggregation of sodium fluorescein in aqueous solutions," *J. Phys. Chem. B*, vol. 115, no. 44, pp. 12896–12904, 2011.

[27] L. Sharma, K. D. P. Nigam, and S. Roy, "Single phase mixing in coiled tubes and coiled flow inverters in different flow regimes," *Chem. Eng. Sci.*, vol. 160, no. April 2016, pp. 227–235, 2017.

[28] S. Klutz, S. K. Kurt, M. Lobedann, and N. Kockmann, “Narrow residence time distribution in tubular reactor concept for Reynolds number range of 10–100,” *Chem. Eng. Res. Des.*, vol. 95, pp. 22–33, 2015.

[29] A. K. Saxena and K. D. P. Nigam, “Coiled configuration for flow inversion and its effect on residence time distribution,” *AIChE J.*, vol. 30, no. 3, pp. 363–368, 1984.

[30] R. N. Trivedi and K. Vasudeva, “Axial dispersion in laminar flow in helical coils,” *Chem. Eng. Sci.*, vol. 30, no. 1, pp. 317–325, 1975.

[31] A. A. Aider, S. Skali, and J. P. Brancher, “Laminar-turbulent transition in Taylor-Dean flow,” *J. Phys. Conf. Ser.*, vol. 14, pp. 118–127, 2005.

[32] K. C. Cheng, R.-C. Lin, and J.-W. Ou, “Fully Developed Laminar Flow in Curved Rectangular Channels,” *J. Fluids Eng.*, vol. 98, no. 1, pp. 41–48, 1976.

[33] M. E. Davis and R. J. Davis, “Chapter 8 Nonideal Flow in Reactors,” in *Fundamentals of Chemical Reaction Engineering*, McGraw-Hill Higher Education, 2003, pp. 260–285.

[34] H. S. Fogler, “Chapter 14 Models for Nonideal Reactors,” in *Elements of Chemical Reaction Engineering*, Fourth Edi., Pearson Education, Inc., 2006, pp. 945–1006.

[35] M. Martinelli and V. Viktorov, “Modelling of laminar flow in the inlet section of rectangular microchannels,” *J. Micromechanics Microengineering*, vol. 19, p. 025013, 2009.

[36] C. Gutierrez, E. Dias, and J. Gut, “Residence time distribution in holding tubes using generalized convection model and numerical convolution for non-ideal tracer detection,” *J. Food Eng.*, vol. 98, no. 2, pp. 248–256, 2010.

[37] P. B. Howell, D. R. Mott, J. P. Golden, and F. S. Ligler, “Design and evaluation of a Dean vortex-based micromixer.,” *Lab Chip*, vol. 4, pp. 663–669, 2004.

[38] E. Mielke, S. S. Mongeon, C. Aellig, P. Plouffe, A. Macchi, and D. M. Roberge, “Micro-Reactor Mixing Unit Interspacing for Fast Reactions in Liquid-Liquid Systems,” *Intern. Doc.*, 2017.

[39] C. P. Holvey, D. M. Roberge, M. Gottsponer, N. Kockmann, and A. Macchi, “Pressure drop and mixing in single phase microreactors: Simplified designs of micromixers,” *Chem. Eng. Process. Process Intensif.*, vol. 50, no. 10, pp. 1069–1075, 2011.

[40] E. Mielke, D. M. Roberge, and A. Macchi, “Microreactor mixing-unit design for fast liquid—liquid reactions,” *J. Flow Chem.*, vol. 6, no. September, pp. 1–9, 2016.

[41] A. P. Torres and F. A. R. Oliveira, “Residence time distribution of liquids in a continuous tubular thermal processing system part II: Relating hold tube efficiency to processing conditions,” *J. Food Eng.*, vol. 35, no. 98, pp. 165–175, 1998.

[42] L. S. Han, “Hydrodynamic Entrance Lengths for Incompressible Laminar Flow in Rectangular Ducts,” *J. Appl. Mech.*, vol. 27, p. 403, 1960.

[43] S. R. L. Gobert, S. Kuhn, L. Braeken, and L. C. J. Thomassen, “Characterization of Milli- and Microflow Reactors: Mixing Efficiency and Residence Time Distribution,” *Org. Process Res. Dev.*, vol. 21, no. 4, pp. 531–542, 2017.

[44] T. Wellsandt, B. Stanisch, and J. Strube, “Characterization Method for Separation Devices Based on Micro Technology,” *Chemie Ing. Tech.*, vol. 87, no. 1–2, pp. 150–158, 2015.

[45] H. Nagasawa and K. Mae, “Development of a New Microreactor Based on Annular Microsegments for Fine Particle Production,” *Ind. Eng. Chem. Res.*, vol. 45, no. 7, pp. 2179–2186, Mar. 2006.

[46] N. Kockmann, J. Kastner, and P. Woias, “Reactive particle precipitation in liquid microchannel flow,” *Chem. Eng. J.*, vol. 135, no. SUPPL. 1, pp. 110–116, 2007.

[47] C.-H. Choi, Y.-W. Su, and C. Chang, “Effects of fluid flow on the growth and assembly of ZnO nanocrystals in a continuous flow microreactor,” *CrystEngComm*, vol. 15, no. 17, p. 3326, 2013.

[48] F. Castro, S. Kuhn, K. Jensen, A. Ferreira, F. Rocha, A. Vicente, and J. A. Teixeira, “Continuous-flow precipitation of hydroxyapatite in ultrasonic microsystems,” *Chem. Eng. J.*, vol. 215–216, pp. 979–987, 2013.

[49] S. L. Poe, M. a. Cummings, M. P. Haaf, and D. T. McQuade, “Solving the clogging problem: Precipitate-forming reactions in flow,” *Angew. Chemie - Int. Ed.*, vol. 45, no. 10, pp. 1544–1548, 2006.

[50] J. Leung, P. Plouffe, and A. Macchi, “Characterization on Effect of Reactor Geometry and Size on the Residence Time Distribution (RTD) of Single Phase Micro-reactor,” *Intern. Rep.*, 2015.

[51] S. S. Mongeon, D. M. Roberge, M. Bittel, P. Elsner, and A. Macchi, “Liquid-Liquid Mass Transfer in an Oscillatory-Flow Mesoscale Coil Reactor without Baffles,” *Org. Process Res. Dev.*, vol. 20, no. 4, pp. 733–741, 2016.